Aerosol Science and Technology, 47:294–309, 2013

ISSN: 0278-6826 print / 1521-7388 online
DOI: 10.1080/02786826.2012.752572

Collection Efficiency of the Aerosol Mass Spectrometer for Chamber-Generated Secondary Organic Aerosols

Kenneth S. Docherty,[1] Mohammed Jaoui,[1] Eric Corse,[1] Jose L. Jimenez,[2] John H. Offenberg,[3] Michael Lewandowski,[3] and Tadeusz E. Kleindienst[3]

[1]*Alion Science and Technology, Research Triangle Park, North Carolina, USA*
[2]*Cooperative Institute for Research in Environmental Sciences (CIRES), University of Colorado, Boulder, Colorado, USA*
[3]*National Exposure Research Laboratory, U.S. Environmental Protection Agency, Research Triangle Park, North Carolina, USA*

The collection efficiency (CE) of the aerosol mass spectrometer (AMS) for chamber-generated secondary organic aerosol (SOA) at elevated mass concentrations (range: 19–207 μg m^{-3}; average: 64 μg m^{-3}) and under dry conditions was investigated by comparing AMS measurements to scanning mobility particle sizer (SMPS), Sunset semi-continuous carbon monitor (Sunset), and gravimetric filter measurements. While SMPS and Sunset measurements are consistent with gravimetric filter measurements throughout a series of reactions with varying parent hydrocarbon/oxidant combinations, AMS CE values were highly variable ranging from unity to <15%. The majority of mass discrepancy reflected by low CE values does not appear to be due to particle losses either in the aerodynamic lens system or in the vacuum chamber as the contributions of these mechanisms to CE are low and negligible, respectively. As a result, the largest contribution to CE in the case of chamber-generated SOA appears to be due to particle bounce at the vaporizer surface before volatilization, which is consistent with earlier studies that have investigated the CE of ambient and select laboratory-generated particles. CE values obtained throughout the series of reactions conducted here are also well correlated with the f_{44}/f_{57} ratio, thereby indicating both that the composition of the organic fraction has an important impact on the CE of chamber-generated SOA and that this effect may be linked to the extent to which the organic fraction is oxidized.

Received 8 August 2012; accepted 7 November 2012.

The authors would like to acknowledge Doug Worsnop and Aerodyne Research, Inc., for the use of a beam width probe which was used to measure beam width dimensions. Jose L. Jimenez was supported by DOE (BER, ASR program) DE-SC0006035 and NASA NNX12AC03G. The U.S. Environmental Protection Agency, through its Office of Research and Development, funded and collaborated in the research described here under Contract EP-D-05-065 to Alion Science and Technology. The article is subjected to external peer review and has been cleared for publication. Mention of trade names or commercial products does not constitute endorsement or recommendation.

Address correspondence to Kenneth S. Docherty, Alion Science and Technology, P.O. Box 12313, Research Triangle Park, NC 27713, USA. E-mail: kdocherty@alionscience.com

[Supplementary materials are available for this article. Go to the publisher's online edition of *Aerosol Science and Technology* to view the free supplementary files.]

1. INTRODUCTION

Atmospheric particulate matter broadly impacts both the environment and human health with the role of particles influenced by both mean particle size and chemical composition. The importance of particle size is highlighted by a strong association between negative environmental and health impacts and the concentration of fine particles (PM_f, typically defined as particles having aerodynamic diameters, d_a, $\leq$2.5 μm [$PM_{2.5}$] or $\leq$1 μm [PM_1]). The role of particle composition, in contrast, is much less well understood due to the complex nature of particle composition as well as its rapid variation in space and time. Recent advancements in aerosol instrumentation and the advent of online analytical methods have provided a means of characterizing fine particle composition with small mass requirements and high-time resolution. The aerosol mass spectrometer (AMS), for example, monitors the bulk chemical composition of nonrefractory submicron particles (NR-PM_1) in real time and complements speciated analysis techniques. The AMS has been used by a large number of research groups around the world to characterize the chemical composition of ambient and laboratory-generated NR-PM_1 (Canagaratna et al. 2007).

The AMS acquires mass spectra of NR-PM_1 from which the concentration of major component species (i.e., organics, nitrate, sulfate, ammonium, and chloride) are derived through the use of spectral fragmentation tables (Allan et al. 2004) and high-resolution spectral analysis in the case of high-resolution time-of-flight AMS data (DeCarlo et al. 2006). AMS total and component species mass concentrations are typically lower than complementary measurements obtained from collocated $PM_{2.5}$

instruments, particularly when sampling ambient particles, due to both the relatively smaller range of particle sizes effectively sampled by the AMS and the presence of refractory material (i.e., those compounds that do not volatilize sufficiently fast at standard AMS vaporizer temperatures to be detected) in ambient aerosols (Docherty et al. 2011). However, even when accounting for these potential sources of discrepancy, AMS reported mass continues to be lower than complementary measurements. As a result, the application of a collection efficiency (CE) factor to AMS data is required to obtain quantitative agreement between the AMS and collocated measurements. Comparisons of AMS and collocated measurements from polluted urban locations have consistently found that a CE = 0.5 is required to obtain quantitative agreement (Canagaratna et al. 2007 and references therein). Cross et al. (2009) also verified a CE = 0.5 using an *in situ* technique when sampling in the vicinity of Mexico City using a high-resolution aerosol-mass spectrometer equipped with a light-scattering unit that optically counts particles during their transit in the particle time-of-flight (PToF) chamber. These results indicate that, on average, the AMS measures half of the ambient PM_f mass reported by other instruments and AMS measurements must therefore be doubled in order to achieve inter-instrument agreement. The CE of laboratory-generated particles has been shown to vary depending on the type of particle (Matthew et al. 2008), but little is known about the CE of chamber-generated SOA.

AMS CE can be expressed via Equation (1) (Huffman et al. 2005) as the product of several terms that individually represent a particular efficiency with which particles sampled by the AMS result in measurable signal at the mass spectrometer.

$$CE = E_L \times E_S \times E_B \quad [1]$$

E_L and E_S represent the efficiency with which particles are transmitted through the aerodynamic lens system and the particle time-of-flight (PToF) chamber, respectively. Together, the product of $E_L \times E_S$ represents those particles that enter the instrument but do not impact the vaporizer surface due to either their impaction or diffusion inside the lens or their high angular divergence in the vacuum chamber. The mass associated with these particles goes undetected by the AMS as a result. E_B, in contrast, represents the fraction of particles that are transmitted to the vaporizer surface with unit efficiency but are not in contact with that surface for long enough to be volatilized at the normal operating temperature of the vaporizer. This effect is commonly referred to as particle "bounce" and results in the AMS not detecting the mass associated with those particles. Each of these efficiencies is dependent on particular aspects of individual particles. For example, E_L is influenced primarily by particle size (Zhang et al. 2004; Liu et al. 2007), E_S by particle morphology and size (Huffman et al. 2005), and E_B by particle phase (i.e., whether the particle is solid or liquid) and volatility (Matthew et al. 2008).

The AMS aerodynamic lens system consists of a cylindrical tube in which a series of axisymmetrical cylindrical constrictions compress the gas and particle trajectories resulting in the focusing of particles within a given size range into a tightly focused particle beam. In general, E_L for the AMS lens system is close to unity for typical accumulation mode particles and allows for the measurement of quantitative mass loadings for particles within this size range (Liu et al. 2007; Bahreini et al. 2008; Takegawa et al. 2009). Accordingly, the contribution of E_L to CE is negligible for these particles and can be virtually eliminated in the case of laboratory-generated particles by size-selecting monodisperse aerosols within the window of optimal lens transmission efficiency. Under ambient sampling conditions, however, E_L can have higher contributions to CE due to the presence of particles near 1 μm or larger as the lens transmission efficiency decreases significantly for particles in this size range. Due to their relatively high inertia, these particles have a higher incidence of impaction on the interior surfaces of the lens system (Zhang et al. 2004). Although small particles (e.g., $d_m < 100$ nm) can also be associated with lower E_L values, these particles do not substantially contribute to CE due to their relatively small mass. Once the particle beam exits the lens system and enters the vacuum chamber, small radial velocity components due to imperfect focusing and Brownian motion cause slight broadening of the particle beam as it travels through the PToF chamber giving rise to the E_S term of CE. Broadening is accentuated in the case of irregularly-shaped particles due to "lift" forces acting on the particle surface. In the majority of cases, E_S appears to have small or negligible contributions to the CE of laboratory-generated (Huffman et al. 2005) and ambient (Delia 2004; Weimer et al. 2006; Salcedo et al. 2007) particles.

Laboratory studies that allow for the contributions of both E_L and E_S to be eliminated indicate that the bulk of AMS CE is contributed by particles bouncing from the vaporizer surface prior to volatilization. Particle bounce is particularly pronounced in the case of solid particles but may also be moderated by particle volatility. Matthew et al. (2008), for example, measured the CE of pure and modified ammonium sulfate (AS) particles. Pure AS particles were modified by increasing the mass fraction of more volatile ammonium nitrate (AN), increasing the relative humidity (RH) of the sampling line, and by condensation of a liquid organic layer. In general, the CE of dry, solid AS particles increased from its minimum of ~25% to unity as either the AN/AS mass ratio, the water/total mass ratio above the AS deliquescence point, or the thickness of liquid organic (dioctylsebacate, DOS) layer are increased. In the case of increased humidity and the presence of a DOS layer, increases in CE observed by Matthew et al. (2008) were likely due to a change in particle phase from solid to liquid which increases the inelasticity of the particle's collision with the vaporizer surface. The phase of mixed AN/AS particles is less clear and could suggest that CE can also be moderated by increasing the volatility of the bulk particle. The results of Cross et al. (2009) also indicate that the CE of ambient particles arises from bounce of particles from the vaporizer surface prior to volatilization.

Various parameters related to particle chemical composition influence E_B through their influence on particle phase. Quinn

et al. (2006) reported that acidified sulfate particles had increased CE relative to pure AS and proposed a parameterization to quantify this effect. As previously discussed, Matthew et al. (2008) found that the CE of laboratory-generated particles that bounce can be influenced by the RH of the sampling line and the resulting water content of particles, the mass fraction of AN, and the presence of a liquid organic layer. Middlebrook et al. (2012) recently investigated the influence of each of these parameters in several ambient AMS datasets and proposed updated parameterizations for the effects of high AN or acidified sulfate particles on CE.

Despite the considerable efforts behind understanding what the AMS CE represents and how it is influenced by physical or chemical properties of various particle types, less is known about whether and to what extent the organic fraction impacts AMS CE. Studies conducted to date suggest that the CE of predominantly organic particles is determined by particle phase (liquid vs. solid), as expected. For example, Alfarra (2004) investigated six pure organic particle standards and found substantially different behavior with respect to CE. One group of organics (DOS, oleic acid, and nonylaldehyde) was associated with a CE of unity while CE values for another group (myristic acid, succinic acid, and pyrene) ranged from 20–50% (Alfarra 2004). Although the chemical nature of each of these compounds varies widely, CE values correlated with organic phase at room temperature and pressure: the constituents of the high CE group were liquids and those with lower CE were solids. Multiple ambient studies have concluded that CE ~0.5 for ambient OA (Salcedo et al. 2006; Aiken et al. 2009). Middlebrook et al. (2012) studied this effect systematically and found that ambient OA in two different environments did not appear to lead to significant deviations from CE ~0.5 value, even when this OA represented a very large mass fraction of NR-PM_1 in two different studies.

The findings of Alfarra (2004) clearly establish a role for organic composition and phase in determining the CE of pure organic standards. Based on the consistency of CE values for ambient OA, this role appears to be diminished in the case of ambient aerosols where the organic fraction is potentially comprised of thousands of different compounds. The question remains whether and to what extent a complex organic matrix influences CE, particularly in light of recent experimental evidence indicating that chamber-generated and ambient secondary organic aerosol (SOA) can exist as solid particles under conditions relevant to the atmosphere (Virtanen et al. 2010, 2011). This is especially important in the case of SOA generated in environmental smog chamber reactions which are typically dominated by a complex organic mass fraction with little if any inorganic components. Bahreini et al. (2005), for example, reported that condensation of chamber SOA onto a pure AS seed particle could lead to an increase or decrease of the CE versus the pure AS seed, and inferred that chamber SOA could be liquid or solid, depending on the precursor and reaction. However, at present there is no predictive understanding of the physical or chemical properties that control the phase and CE of chamber SOA.

Here, we investigate the CE of SOA formed from the reaction of a number of parent hydrocarbon/oxidant combinations and also of pure organic standards by comparing measured AMS mass concentrations with collocated measurements from a scanning mobility particle sizer (SMPS), a Sunset semi-continuous carbon monitor (Sunset), and gravimetric filter measurements. Obtained CE values varied widely from an average minimum of ~20% to 100% and are likely driven primarily by bounce of particles from the vaporizer surface. A range of CE values for chamber-generated SOA suggests that the phase of particles range from liquid-solid mixtures to solid inside the AMS. CE of chamber-generated SOA is relatively insensitive to the RH of the sampling line, the mass fraction of AS seed, and the mass fraction of nitrate (presumably organic nitrate) but is inversely proportional to the ratio of f_{44}/f_{57} with relatively high correlation suggesting that the balance of oxidized and reduced constituents in various organic aerosols has a strong influence on particle phase of chamber SOA.

2. EXPERIMENTAL

2.1. Secondary Organic Aerosol (SOA) Production

SOA was generated in most experiments through the oxidation of hydrocarbons by either the hydroxyl (OH) or nitrate (NO_3) radicals or ozone (O_3). In a limited number of experiments, hydrocarbon standards including dioctyl sebacate (DOS) and azelaic acid were introduced into the reaction chamber in the absence of oxidants either via atomization or evaporation. Details of each experiment considered here are presented in Table S1. All reactions were conducted in and aerosol was sampled from a 14.5 m^3 fixed volume, Teflon-coated reaction chamber operated in dynamic mode (Edney et al. 2005) with a residence time of 4 h. Operating the chamber in dynamic mode produces steady-state conditions wherein SOA concentrations and chemical composition are relatively stable over extended periods. Overall, stable aerosol concentrations were maintained during each experiment over the course of 4–5 days. With respect to the reactions considered in the current analysis, OH was generated through irradiation of either methyl nitrite (presence of NO_x) or hydrogen peroxide (absence of NO_x) using a combination of blacklights and ultraviolet (UVA in high NO_x experiments and also UVB in low NO_x experiments) lamps in order to provide a radiation spectrum (λ = 300–400 nm) similar to that of solar radiation to the extent possible, NO_3 was generated through thermal decomposition of dinitrogen pentoxide, and O_3 was produced from a low flow of clean air flowing around a germicidal mercury bulb in a quartz sleeve. Prior to the start of each experiment, polydisperse seed particles (e.g., AS, AN, and NaCl) were atomized into the chamber with a TSI, Inc. (St. Paul, MN, USA) single jet atomizer (model no. 9302) resulting in average seed particle mass concentrations of 2.32(±1.54)

μg m^{-3} with a median volume diameter ~80 nm and atomization was continued throughout the course of each experiment. The organic-to-inorganic volume and mass ratios during CE evaluation periods for each reaction are provided in Table S1. Overall, SOA generated during each reaction was found to contribute the overwhelming majority of particle volume (>85% in each case) and mass (>75% in each case). Finally, each reaction was conducted under dry conditions (typically 1–5% RH on average) with the exception of a few that were conducted in the presence of added water vapor (typically 25–35% RH on average; maximum RH of 45% for a single reaction). Mass concentrations of SOA generated throughout the set of experiments considered here varied widely (range: 19–207 μg m^{-3}) but were high overall with an average (standard deviation) of 64 μg m^{-3} (43 μg m^{-3}).

2.2. Quadrupole Aerosol Mass Spectrometer (AMS) Measurements

Throughout each experiment, the average composition and concentration of NR-PM$_1$ was monitored using a quadrupole AMS. The instrument can operate in two modes depending on the operation of a chopper wheel located downstream of the aerodynamic lens exit. In mass spectral (MS) mode, the position of the chopper wheel is alternated between open (thereby producing a spectrum of particle-associated species and background gases) and closed (to collect the spectrum of background gases only). In PToF mode, the particle beam is intermittently chopped allowing a discrete packet of particles to proceed past the chopper. The speed with which particles exit the lens system is size-dependent with higher speeds being associated with smaller particles. The size-dependent velocity of particles within the discrete aerosol packet allows the AMS to measure particle size distributions. In this study, the AMS was alternated between MS and PToF modes every 30 s continuously throughout each experiment to obtain both average mass spectra and size distributions for chamber aerosol, the duration of both open and closed MS period was 15 s, and a 2% duty cycle chopper wheel was operated at a frequency of 160 Hz.

Aerosol was sampled from the chamber to the inlet of the AMS through stainless steel tubing using a bypass flow of 1.0 l min^{-1} to decrease the residence time in the sampling line (estimated to be on the order of 16 s). Additionally, a combination of a Stratos tube mixer (Cole-Parmer, Mod. 04669–52) and an isokinetic sampling inlet upstream of the bypass flow exit were used to ensure mixing of the sampling stream in the line prior to its introduction into the AMS, which sampled at a rate of 0.1 l min^{-1}.

Average mass spectra and particle size distributions were collected every 5–10 min depending on the experiment. Analysis of AMS data was performed using the standard Q-AMS Analysis Toolkit (v. 1.41), which incorporates the analysis algorithms of Allan et al. (2003), Jimenez et al. (2003), and Allan et al. (2004). To account for instrument-specific fragmentation patterns and the contributions of gas-phase species that are dependent on the specific sampling environment (Allan et al. 2004), the mass spectral fragmentation table for each analysis was modified using mass spectra obtained during periods both prior to and following each experiment when HEPA-filtered chamber air was sampled into the instrument.

Finally, the ionization efficiency (IE_{NO3}) of the AMS (Jayne et al. 2000) was calibrated with monodisperse AN particles intermittently throughout the series of chamber experiments conducted here (see Figure S1 in the online supplemental information). IE_{NO3} decreased in proportion to the m/z 28 signal (air beam, AB) resulting in a relatively constant IE_{NO3}/AB ratio throughout the sampling interval. Decreases or changes in IE_{NO3} were attributed to typical degradation of detector sensitivity or a change in the ionizer filament which was changed due to a failure. IE_{NO3} values used during each experiment are indicated in Figure S1. A CE of unity was also used during analysis of AMS data.

2.3. Scanning Mobility Particle Sizer Measurements

Particle number distributions were also monitored throughout each experiment by a TSI (St. Paul, MN, USA) SMPS system consisting of a model 3071 classifier and model 3010 condensation particle counter. Aerosol and sheath flow rates for the SMPS were 0.25 l and 2.0 l min^{-1}, respectively. As with the AMS, aerosol was drawn from the chamber to the SMPS system through stainless steel tubing at a volume flow rate of 0.25 l min^{-1} resulting in a residence time of approximately 90 s. Particle volume distributions were calculated from number distributions assuming spherical geometries over the entire range of particle sizes.

Volume concentrations must be converted to mass concentrations before comparison with AMS mass concentration is possible. Particle density is highly variable depending on the various constituents of the aerosol and few widely available techniques provide explicit density measurements (McMurry 2000). Here, we use the average bulk particle density obtained from linear regression of filter-based mass versus SMPS volume measurements in order to convert particle volume distributions to mass distributions (Figure 1a and discussion below).

2.4. Sunset Semi-Continuous Organic Carbon Measurements

Organic carbon (OC) mass concentrations were monitored hourly throughout each experiment using a Sunset (Tigard, OR, USA) semi-continuous carbon monitor (Sunset). Aerosol was sampled through stainless steel tubing at a flow rate of 8 l min^{-1} resulting in a residence time of approximately 3 s. An inline carbon-impregnated denuder was used upstream of the Sunset to reduce the condensation of gas-phase species on the filter. The background of the instrument was checked both prior to and following each experiment by measuring the response of the instrument to particle-free clean air sampled directly from the clean air system and was used to correct OC measurements made during each experiment. The measured Sunset background

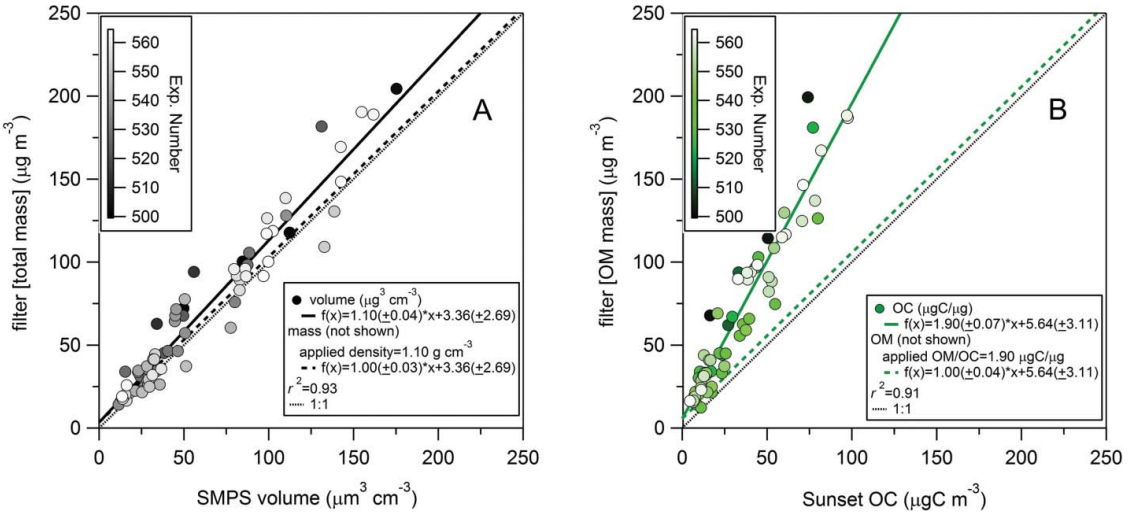

FIG. 1. Scatter plots of (a) filter total mass concentration versus SMPS particle volume concentration and (b) filter OM mass concentration versus Sunset OC concentrations. Data points are shaded by experiment number here and in subsequent plots simply to highlight the even distribution of data obtained throughout the sampling interval. The results of linear regression in each case are also shown and indicate average particle density (a) and OM/OC (b) values. Displayed regression results (dashed lines) in (a) and (b) are those obtained by comparing filter- versus SMPS-based mass (converted using a bulk density of 1.10 g cm^{-3}) and filter- versus Sunset-based OM (converted using OM/OC of 1.90 $\mu gC\ \mu g^{-1}$), respectively. (Color figure available online.)

was 2.75 (±0.97) $\mu g\ m^{-3}$ on average or 7.3 (±6.5)% of post-reaction OC measurements.

2.5. Filter Sampling

Filter samples were collected periodically throughout the course of each chamber experiment for gravimetric determination of chamber particle mass concentration and offline speciated analysis. In most cases, duplicate or triplicate filter samples were collected in cartridges using 47 mm Pall-Gelmann (Port Washington, NY, USA) teflon-impregnated glass fiber filters. Each filter cartridge was located downstream of a carbon-impregnated diffusion denuder to remove gas-phase and semi-volatile species and a Tylan (San Diego, CA, USA) model FC 262 mass flow controller was used to control the mass flow rate ($\sim 0.96 \pm 0.12\ m^3\ h^{-1}$) over the duration of sampling (typically 24 h). The particle mass collected on each filter was determined gravimetrically using a Mettler-Toledo (Columbus, OH, USA) UMX2 microbalance as the difference between the final and initial filter weight. The average mass, sampling line flow rate, and duration of collection for each set of filters were used to calculate chamber particle mass concentrations using Equation (2):

$$\text{filter [total]}\ (\mu g\ m^{-3}) = \text{filter mass}\ (\mu g)/(\text{flow rate}\ (m^3\ hr^{-1})^* \times \text{sampling duration (hr)}) \quad [2]$$

The average filter mass measurements described above represent total particle mass (i.e., including inorganic and organic material [OM]) and are suitable for comparison with SMPS volume concentrations. Filter-based OM mass concentrations were derived by subtracting the contribution of inorganic seed to filter-based total mass concentrations obtained form Equation (2) in order to compare with corresponding Sunset OC measurements. As shown in Equation (3), the inorganic mass contribution was calculated as the product of seed volume concentrations obtained from the SMPS prior to the initiation of each reaction (i.e., V_{seed}) and the corresponding inorganic seed density (i.e., ρ_{seed}).

$$\text{filter [OM]}(\mu g\ m^{-3}) = \text{filter [total]}(\mu g\ m^{-3}) - [(V_{seed})(\mu m^3 cm^{-3}) \times \rho_{seed}(g\ cm^{-3})] \quad [3]$$

3. RESULTS AND DISCUSSION

3.1. Consistency of Filter, SMPS, and Sunset Measurements

As each of the filter, SMPS, and Sunset measurements is associated with potential uncertainties, we evaluate the consistency among these measurements prior to their application in estimating AMS CE values. Total particle mass concentrations calculated from filter weights for each sampling period are plotted against corresponding SMPS volume concentrations in Figure 1a while particle organic material (OM) concentrations calculated from filter weights are similarly plotted against corresponding Sunset OC measurements in Figure 1b. In each plot, data points are shaded according to the order in which the experiment was conducted (i.e., experiment number) to illustrate the even distribution of density and OM/OC values along the full range of experiments and the absence of systematic drift which

could bias either the filter, SMPS, or Sunset measurements as a function of time.

As Figure 1a shows, total filter mass concentrations are consistent with corresponding SMPS volume concentrations throughout the range of experiments. On average, filter concentrations are slightly higher than corresponding volume concentrations which is indicative of an average particle density >1 g cm^{-3}. The slope obtained from linear regression of total filter concentration versus SMPS volume concentration provides an average particle density of 1.10 (±0.04) g cm^{-3} along with a small intercept of 3.36 (±2.69) μg m^{-3} which could represent either larger filter measurements relative to the SMPS (e.g., via small contributions of gas-phase or semi-volatile species) or visa versa (e.g., via partial evaporation of particles in the classifier). The value of the intercept in this case is <5% of the average total filter mass concentration over the entire range of all of the experiments, which is within the combined error of both measurements and filter mass concentrations are highly correlated with SMPS volume concentrations with $r^2 = 0.93$. Filter OM concentrations are also highly correlated with Sunset OC concentrations ($r^2 = 0.91$) and the slope obtained from linear regression indicates an average OM/OC ratio of 1.90 (±0.07) μg/μgC for the entire set of experiments. Again a small intercept of 5.64 (±3.11) is ∼8% of the overall average filter OM concentration and is within the combined error of both measurements. The small intercepts in each case could be due to filter artifacts, particularly in those reactions with relatively highly oxidized SOA. While a detailed discussion of filter sampling artifacts is beyond the scope of the current work, it is worthwhile to note that the magnitude of these errors is within the error of the combined measurements. Additionally, these potential errors do not likely contribute significantly to the overall conclusions of this work due to our use of average density and OM/OC values and several independent measurements to calculate CE.

The average density and OM/OC values obtained here are similar to available literature values for ambient and laboratory-generated aerosols. For example, Turpin and Lim (2001) used literature data to arrive at a recommended density of 1.2 g cm^{-3} for ambient particulate OM. This value also is similar to density estimates of various chamber-generated SOA types (1.30 ± 0.07 g cm^{-3}; Table S2) comparable to those of the current study. The reason the average density obtained here is slightly lower than the recommended ambient value is unknown but could be likely related to lower O/C ratios obtained for chamber-generated SOA, especially at the relatively high concentrations used here (Chhabra et al. 2010) and the proportionality between O/C ratio and density (Kuwata et al. 2012). Recommended OM/OC values for ambient aerosol range from 1.6 (±0.2) μg/μgC for urban aerosols to 2.1 (±0.2) μg/μgC for aerosols in nonurban regions (Turpin and Lim 2001), which is similar to the range for chamber-generated SOA (1.5–2.15 μg/μgC, ref. Table S3) based on elemental analysis of high-resolution AMS data (Aiken et al. 2008). It is worth noting that the OM/OC value obtained by linear regression is only slightly higher than the median of either the recommended ambient range of Turpin and Lim (2001) or the range of measured values for chamber-generated SOA presented in Table S3. Table S3 and Figure S5 also compare OM/OC values calculated using filter OM/Sunset OC measurements (OM/OC_{filter}) with those obtained from AMS measurements (OM/OC_{AMS}) both based on f_{44} alone (Aiken et al. 2008) and when AMS NO_2 moieties contribute to OM. Overall, OM/OC_{filter} measurements are higher than both OM/OC_{AMS} values with the latter tending to have better agreement with previously published values. The lack of closure between non-AMS and AMS OM/OC values, particularly when NO_2 moieties are included in OM/OC_{AMS}, suggests that the difference in the two ratios is not likely due to the fact that OM/OC_{AMS} as calculated here (i.e., using unit resolution spectra) does not include contributions of NO_2 moieties to OM (Farmer et al. 2010) and suggests that either artifacts associated with either filter OM or Sunset OC measurements, and/or other potential biases in the AMS measurement are responsible for the difference.

The high degree of correlation between each corresponding measurement suggests the absence of a substantial bias in the SMPS and Sunset data relative to the filter measurements. Despite the high degree of correlation, some variability (or noise) continues to exist which can distort calculated CE values depending on which measurement the AMS data is compared with, thereby making it more difficult to observe larger trends that can potentially exist between particle composition and resulting AMS CE. We use the average density and OM/OC values obtained by linear regression to convert SMPS volume to mass and Sunset OC to OM, respectively, prior to their comparison with corresponding AMS measurements in order to minimize these small variations and their impact on calculated CE values.

3.2. Comparison of AMS Measurements with Filter, SMPS, and Sunset Measurements

AMS CE can be evaluated through the change in measured sulfate concentrations prior to the onset of SOA formation and following the condensation of SOA on AS seed particles (Bahreini et al. 2005). At high-SOA mass concentrations such as those observed here, however, the contribution of OA to reported sulfate concentrations is difficult to fully resolve with unit resolution spectra and the standard AMS fragmentation table, which can lead to substantial uncertainty as a result. Reliably removing the influence of OA on sulfate mass concentrations under these conditions can only be done well when high-resolution data are available. Due, in part, to these considerations, AMS CE is calculated as the ratio of AMS mass concentration to corresponding filter, SMPS, or Sunset concentrations for each of the reactions conducted here. AMS total and OM concentrations are plotted against corresponding filter values in Figures 2a and b, respectively. AMS concentrations are not plotted versus SMPS total and Sunset OM values in these figures but are similar. Data points in Figures 2a and b have been shaded by

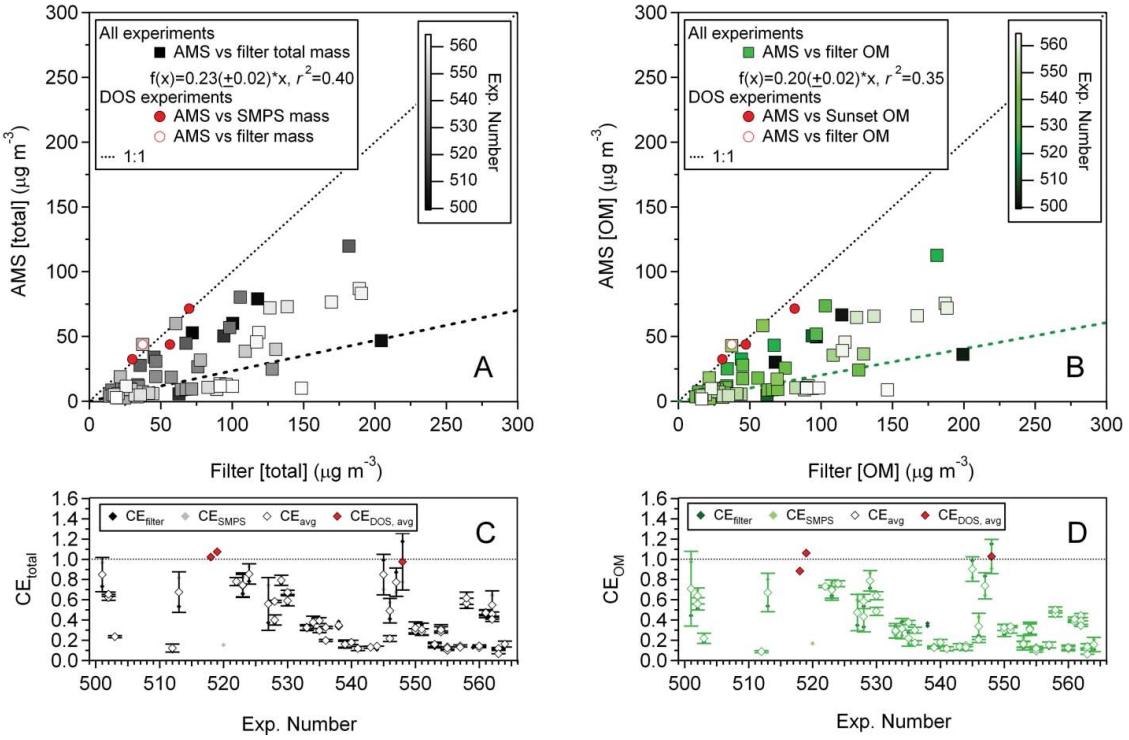

FIG. 2. Comparison of SMPS and AMS total mass concentrations (a) and Sunset and AMS OM concentrations (b) versus the corresponding filter-based measurements. Results of linear regression in each case have been added to show overall trends and to show the correspondence between each measurement. CE values based on each total and OM measurement pair are shown in panels (c) and (d), respectively, along with the overall average. Error bars shown in (c) and (d) correspond to the twice the standard deviation of each CE measurement set. The red data points in these panels reflect CE values for standard DOS particles which were used to ensure the consistency of AMS measurements over time. (Color figure available online.)

experiment number and results of linear regression of AMS against corresponding filter measurements are also shown.

With respect to total mass, AMS measurements are considerably lower than filter measurements and the two are also less well correlated. Linear regression of AMS data versus filter measurements yields a slope of 0.23 (±0.02) with an $r^2 = 0.40$ indicating not only that CE values are much lower than unity on average for the chamber-generated SOA, but that CE also varies widely among the different experiments. As expected based on the small contribution of inorganics to aerosol formed in these reactions, the trend for AMS OM (Figure 2b) is similar to that observed for total mass concentration with the AMS measurements again being considerably lower than (slope = 0.20 ± 0.02) corresponding filter measurements.

Calculated CE values for total particle mass, using both filter and SMPS total mass concentrations, and for particle OM, using both filter and Sunset OM concentrations, are shown in Figure 2c and d, respectively along with average values (e.g., for total mass, $CE_{avg} = [CE_{filter} + CE_{SMPS}]/2$). Error bars associated with each data point correspond to the standard deviation of each CE measurement set. Additionally, CE values for DOS particles are also shown. DOS forms spherical, liquid particles and has previously been determined to have a CE = 1.0 (Alfarra 2004). DOS was used as a standard to evaluate the AMS performance and, more importantly, to ensure that obtained CE values are not a consequence of a change in AMS performance. DOS aerosols were sampled early (ER518 and ER519) and again in the latter half (ER548) of experiments conducted here. CE values for DOS were consistently near unity in each of these experiments which tends to rule out instrumental problems as a potential cause of low CE values observed in other experiments.

As expected due to the dominant contribution of OM to the chamber aerosols, CE_{total} and CE_{OM} values are nearly identical for each of the reactions in the dataset (Figure S2). Overall, average CE values are lower than unity for all experiments, other than a few including the DOS experiments, and highly variable. This variability could be due to either physical or chemical characteristics of the aerosol and the influence of these factors on the various efficiencies (e.g., E_L, E_S, or E_B) associated with CE. In order to assess the potential for SOA composition to influence CE, we must first evaluate the overall contributions of E_L, E_S, and E_B to CE.

3.3. Contributions of E_L, E_S, and E_B to CE of Chamber-Generated SOA

3.3.1. AMS Lens Transmission Efficiency, E_L

Assuming negligible or at least similar particle losses in the sampling lines of each instrument, the AMS aerodynamic lens

system is the first possible cause of measurement discrepancies due to its limited transmission window (Liu et al. 2007) relative to the other techniques. Previous investigations into the CE of laboratory-generated aerosols (Matthew et al. 2008) used monodisperse particles within the window of optimal lens transmission efficiency thereby eliminating the contribution of E_L to CE. In the case of polydisperse chamber-generated SOA, however, a fraction of particle mass may exist outside the window of optimal lens transmission efficiency and E_L must be considered as a potential loss mechanism. While both small and large diameter particles can be associated with low lens transmission efficiency, the loss of large, high-mass particles has a much more profound impact when comparing AMS and other comparable mass-based measurements.

In order to examine the contribution of E_L to calculated CE obtained for each experiment, the lens transmission efficiency (i.e., the transmission efficiency of the lens system as a function of particle size) was evaluated using two different methods: using a polydisperse DOS ($E_{L,\mathrm{DOS}}$) distribution, and; using size-selected, monodisperse AN particles ($E_{L,\mathrm{AN}}$). In general, DOS and AN particles within the optimal lens transmission efficiency window are associated with a CE of unity due to the negligible influences of beam broadening and particle bounce for each type of particle despite the slight deviation of dry AN particle shape from sphericity (Jayne et al. 2000). As a result, any difference in measured particle mass can be attributed to low E_L after the IE of the instrument has been properly calibrated (Jimenez et al. 2003).

$E_{L,\mathrm{DOS}}$ was calculated by comparing AMS and SMPS particle mass distributions for ER518. The SMPS particle volume distribution was converted to mass and d_m was converted to d_{va} using a density of 0.914 g cm^{-3} and a shape factor (X_v) of 1.0 using the following equation (DeCarlo et al. 2004)

$$d_{\mathrm{va}} = d_{ve} \times (\rho_p / X_v) \quad [4]$$

where ρ_p is the density. d_m is equivalent to d_{ve} for spherical particles (Hinds 1999), which is the case for DOS, and the conversion to d_{va} establishes a consistent particle size dimension required to compare AMS and SMPS mass distributions. The absolute intensities (dM/dlogd_m) of all points in both AMS and SMPS distributions were also constrained to vary between zero and one by normalizing each value by the maximum in each distribution. It is important to note that, prior to normalizing, the maximum dM/dlogd_m value from the SMPS (2.14) and dM/dlogd_{va} from the AMS (2.24) were quite similar (not shown). $E_{L,\mathrm{DOS}}$ was then calculated as the ratio of the normalized AMS distribution to that of the SMPS. Both normalized SMPS and AMS mass distributions and $E_{L,\mathrm{DOS}}$ are shown as a function of d_{va} in Figure 3a. In contrast, $E_{L,\mathrm{AN}}$ was evaluated as the ratio of AMS/CPC particle counts for size-selected monodisperse AN distributions over the range 50 nm $> d_m >$ 500 nm. The $E_{L,\mathrm{AN}}$ efficiency curve is also shown in Figure 3a along with an average E_L curve obtained by Liu et al. (2007) ($E_{L,\mathrm{Liu}}$) for reference.

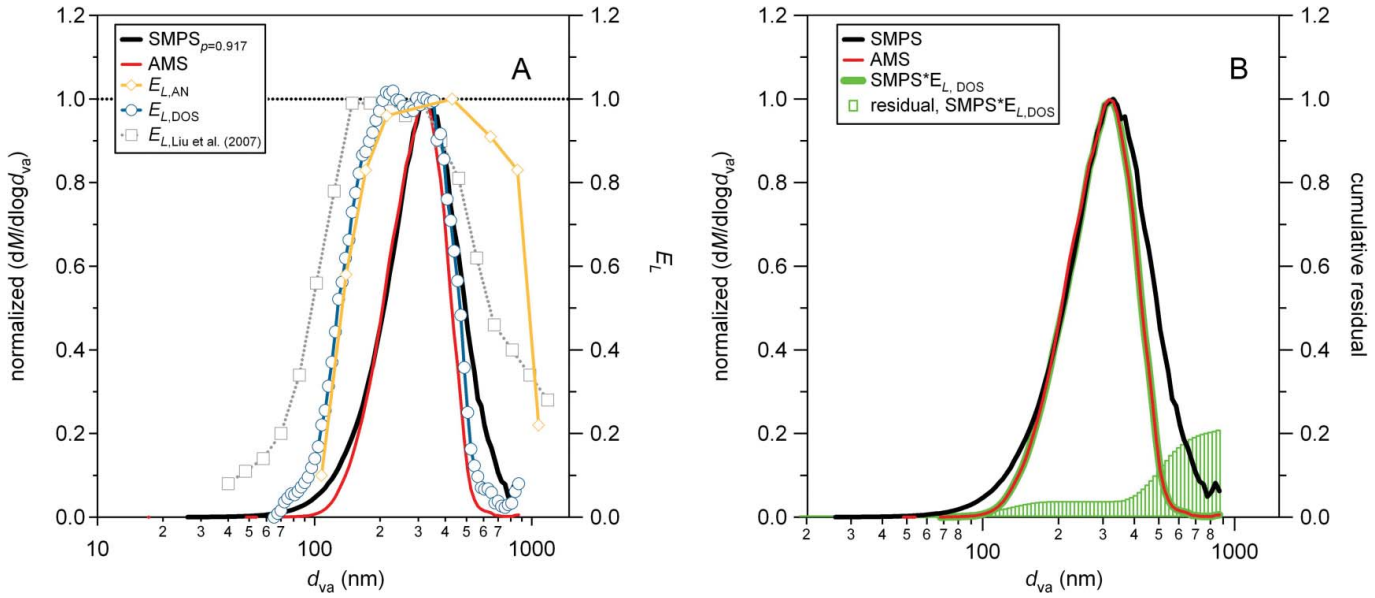

FIG. 3. Investigating E_L and its contribution to CE. (a) shows various E_L curves including $E_{L,\mathrm{DOS}}$ (calculated as the ratio of normalized AMS/SMPS particle size distributions) and $E_{L,\mathrm{AN}}$ (determined using size-selected monodisperse AN particles) as a function of particle diameter (d_{va}). An average E_L curve obtained by Liu et al. (2007) is also shown for reference. AMS and SMPS particle size distributions for DOS particles (ER518) are shown in (b) as along with the adjusted SMPS distribution (SMPS*$E_{L,\mathrm{DOS}}$). The contribution of E_L to CE in each reaction is calculated as the ratio of areas for SMPS $\times$ $E_{L,\mathrm{DOS}}$ and SMPS distributions, shown as the cumulative residual in (b). (Color figure available online.)

Overall, AMS and SMPS mass distributions for DOS are similar over the 200 nm $< d_{va} <$ 350 nm size range and $E_{L,DOS}$ is near unity as a result. SMPS mass is slightly higher for $d_{va} <$ 150 nm and $d_{va} >$ 350 nm particles which is reflected by a precipitous decrease in $E_{L,DOS}$ within each respective size range. In the $d_{va} <$ 150 nm range, there is only a small amount of difference among each of the E_L curves with $E_{L,DOS}$ and $E_{L,AN}$ profiles being very similar. $E_{L,Liu}$ exhibits somewhat better performance toward the smaller end of this range with unit transmission efficiency extending down to $d_{va} \sim$150 nm. The increased efficiency of $E_{L,Liu}$ could be due either to pressure differences between the two lens systems (e.g., due to different orifices or upstream pressure) or to inherent differences between the lens systems which tend to shift the optimum lens transmission efficiency window (Liu et al. 2007).

In the $d_{va} >$ 350 nm range, $E_{L,DOS}$ and $E_{L,Liu}$ are generally similar. However, $E_{L,Liu}$ exhibits somewhat better performance at larger particle diameters as evidenced by the steeper decline in $E_{L,DOS}$ as $d_{va} >$ 350 nm. The performance of $E_{L,AN}$ is better still with unit value transmission efficiency extending to 420 nm and >80% efficiency out to 860 nm. Interestingly, the $E_{L,AN}$ and $E_{L,Liu}$ curves provide a similar transmission efficiency for particles having $d_{va} >$ 1000 nm. This is the most significant difference among of the three E_L profiles with $E_{L,DOS}$ exhibiting the lowest overall transmission efficiency for large particles.

It may be that $E_{L,DOS}$ truly represents the lens transmission efficiency for our particular system. We note, however, that the performance represented by $E_{L,DOS}$ for large diameter particles is uncharacteristically poor compared with that of similar lenses evaluated in previous studies. As a result, we are inclined to believe that the $E_{L,AN}$ profile is more likely to be accurate. The steeper decline of $E_{L,DOS}$ relative to $E_{L,AN}$ could be wholly or in part due to the SMPS overestimating particle mass in the large diameter range. Because volume and mass scale proportionally to the cube of particle diameter, SMPS mass distributions rely heavily on accurate particle number counts. This is particularly true for large particles where small errors in number count can lead to substantial errors in calculated particle mass. In contrast, the impact of counting errors is diminished in the case of $E_{L,AN}$ given the longer sampling time for each particle size. It is difficult to determine with certainty whether the steep decline in $E_{L,DOS}$ is real or due to an artifact. It is worthwhile to note also that in a few cases (see discussion below), the lens transmission efficiency is substantially better than $E_{L,DOS}$ would suggest, particularly for large d_{va} particles. Although this appears to support the contention that the steep decline in $E_{L,DOS}$ is at least partly due to an artifact of the SMPS measurement, we continue to use $E_{L,DOS}$ to estimate the contribution of E_L to CE due to its high spatial resolution and because it provides an upper bound on the contribution of E_L to CE.

A similar procedure was used to estimate the contribution of E_L to CE for each reaction. In this procedure, the SMPS was assumed to accurately represent particle mass distributions which were mapped to d_{va} space by aligning the maximum of both SMPS and AMS distributions and assuming an $X_v =$ 1.0. Although dynamic shape factors are not well known for chamber-generated SOA, they do not appear to deviate significantly from unity based on particle beam width measurements (see discussion below). The SMPS mass distribution was then multiplied by $E_{L,DOS}$ and the contribution of E_L to CE in each case was calculated as the ratio of the difference in area between the original and modified (SMPS$\times E_{L,DOS}$) to the area of the original distribution (i.e., (SMPS – SMPS$\times$ $E_{L,DOS}$.)/SMPS) An example of the calculation is shown in Figure 3b for the polydisperse DOS distribution. As expected, the AMS and modified SMPS distributions appear very similar. The cumulative residual (i.e., $\Sigma_{0\rightarrow i}$ (SMPS$_i$ – (SMPS$\times$ $E_{L,DOS})_i$/SMPS$_i$)), corresponds to the mass fraction lost due to lens transmission inefficiency and is represented by the bars at the bottom of Figure 3b. The cumulative residual for the DOS distribution is 21.1%, and is driven by particles in the large size range. Conversely, a cumulative residual of this magnitude indicates an E_L value on the order of ~80% for this particular polydisperse DOS distribution.

E_L values for distributions obtained from each reaction were evaluated similarly and used to calculate E_L-adjusted CE values (i.e., CE/E_L), in which the influence of E_L on CE has essentially been removed so that the remaining CE value is due to the contributions of $E_S \times E_B$. Raw CE values are plotted versus CE/E_L values in Figure 4 along with the results of linear regression. Application of the $E_{L,DOS}$ transmission curve results in an upper bound average lens transmission efficiency of 74 (±4)% across all reactions indicating relatively minor losses in the AMS lens system. This efficiency increases only slightly to 84 (±5%) if the contribution from the residual between the AMS and SMPS at small particle diameters is removed, reflecting the low contribution of small particles to CE. Each of these slopes, however, may be artificially low due to the presence of a number of outliers (e.g., ER523, ER558, ER561, and ER562) for which CE/$E_{L,}$ is substantially higher than the corresponding CE value suggesting that E_L for these reactions is much lower than for other experiments. AMS and SMPS mass distributions for these reactions along with modified SMPS distributions (by $E_{L,DOS}$) are shown in Figure S3 and are distinguished by the presence of a large fraction of particle mass at diameters larger than the window of optimum lens transmission efficiency. In the case of ER558, ER561, and ER562, the original SMPS distribution shows a large contribution from particles that should be too large to be efficiently transmitted through the lens system according to $E_{L,DOS}$ yet the AMS mass distribution closely resembles the original SMPS distribution. The precise cause of this discrepancy is not known. Possible causes include a simultaneous decrease in the transmission efficiency of large diameter particles in both the AMS and SMPS or the existence of a small fraction of SOA mass that desorbs slowly from the vaporizer surface (Salcedo et al. 2010) thereby broadening the AMS distribution as a result. The coincidence of either of these phenomena with the striking agreement between the

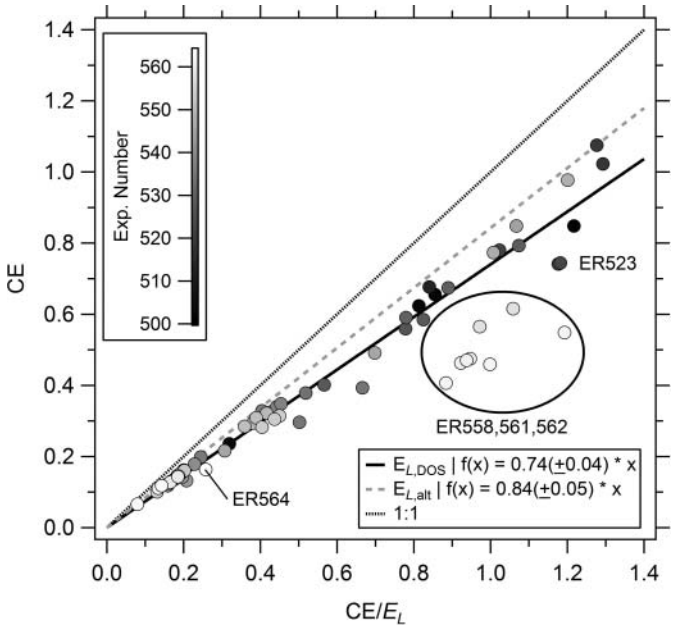

FIG. 4. Scatter plot of CE versus CE/E_L for the range of experiments investigated during this study along with the results of linear regression. On average, E_L is estimated to contribute approximately 26% to CE. A lower bound contribution of approximately 16% is obtained if we assume that the residual between SMPS and AMS size distributions in the range of small particle diameters results from a measurement artifact (see text). CE and CE/E_L values are highly correlated with the exception of outliers ER523, ER558, ER561, and ER562 (labeled in figure) where the contribution of E_L appears to be overestimated due to large particle size distributions (see text and Figure S3).

distributions would, however, be remarkable. Although the precise cause is unclear, the modified SMPS distribution in each case considerably underestimates both particle mass relative to the AMS and E_L. In contrast, the modified SMPS distribution for ER523 closely resembles the AMS mass distribution indicating an appropriate E_L value. With regard to the other distributions within this set, however, the application of $E_{L,\mathrm{DOS}}$ clearly underestimates E_L and overpredicts CE/E_L as a result. If these outliers are removed from the fitting routine, the average lens transmission efficiency using the $E_{L,\mathrm{DOS}}$ curve increases slightly to 76 (±5)%.

3.3.2. *Efficiency Due to Particle Beam Broadening, E_S*

E_S values have been measured for a variety of laboratory-generated (Jayne et al. 2000; Huffman et al. 2005) and ambient (Salcedo et al. 2005, 2007; Weimer et al. 2006) aerosols by using a particle beam width probe (BWP) designed to measure the width of the particle beam near the surface of the heated vaporizer. In each case, E_S for a wide variety of particle types was found to be near unity indicating that irregular particle shape and potential beam broadening have negligible contributions to CE. While a BWP was not available during the experiments conducted for this analysis, one was acquired and used to evaluate the beam width dimensions for AS, DOS-coated AS, and SOA formed in a reaction duplicating the conditions of ER539 (napthalene photooxidation), which had one of the lowest CE/E_L values (18%) within the range of experiments performed here.

BWP profiles for these particle types are shown in Figure 5. The average fraction of particle mass blocked by the BWP during its traverse across the vaporizer surface is shown for each of the main particle species in naphthalene SOA as well as for total mass. Error bars associated with each of these data points correspond to the standard deviation of AMS data. The attenuation of the total particle mass was also converted to a transmission curve using the method of Huffman et al. (2005) to show the overall beam dimensions. Beam dimensions for naphthalene SOA, as well as those for AS and DOS-coated AS particles are shown in Figure 5 along with the calculated beam width parameters for the SOA particle beam. As discussed in Huffman et al. (2005), a solid angle of detection (Ω, in steradians) $<9.3 \times 10^{-5}$ leads to an E_S of unity for the AMS "short chamber" which was used for the experiments discussed here. The dimensions of the particle beam obtained from naphthalene photooxidation SOA ($\Omega = 1.8 \times 10^{-6}$) indicate that the contribution of E_S is negligible, which is consistent with earlier beam width measurements. This result is consistent with a visual comparison of beam dimensions obtained for the SOA and spherical DOS-coated AS particles. The width of the naphthalene SOA beam is only slightly wider that of the DOS-coated AS particles. These observations support our earlier assumption of SOA shape factors ∼1.0. They also indicate a negligible contribution of beam broadening to CE consistent with earlier findings. Accordingly, we assume that $E_S = 1$ for SOA generated from the experiments conducted here.

3.4. Origins of CE for Chamber-Generated SOA

The influence of many factors shown to impact CE for ambient particles should be minor for chamber-generated SOA given the dominance of SOA and small contributions from inorganic material. For example, the water content of chamber-generated SOA is not likely to substantially influence CE. While chamber-generated SOA can be slightly hygroscopic under atmospheric conditions, particularly after extensive aging (Varutbangkul et al. 2006; Prenni et al. 2007; Engelhart et al. 2008; Duplissy et al. 2011), the RH of chamber reactions is typically insufficient to partition substantial water on SOA, and much of the particle-associated water may be lost after sampling into the AMS vacuum system (Zelenyuk et al. 2006; Matthew et al. 2008). RH was ≤45% for all reactions conducted here and was considerably lower (∼1–5%) during the majority of reactions that were not conducted in the presence of added water vapor. Even in the case of highly hygroscopic particles, such as inorganic or ionic solids, an RH > 50–60% is typically required to condense appreciable amounts of water. As a result, the CE of chamber-generated SOA considered here should be fairly insensitive to RH which appears to be the case. CE values are plotted against measured chamber RH in Figure S4a, which suggests that CE values are not sensitive to RH. If RH were a principle determinant of CE, one would reasonably expect to observe

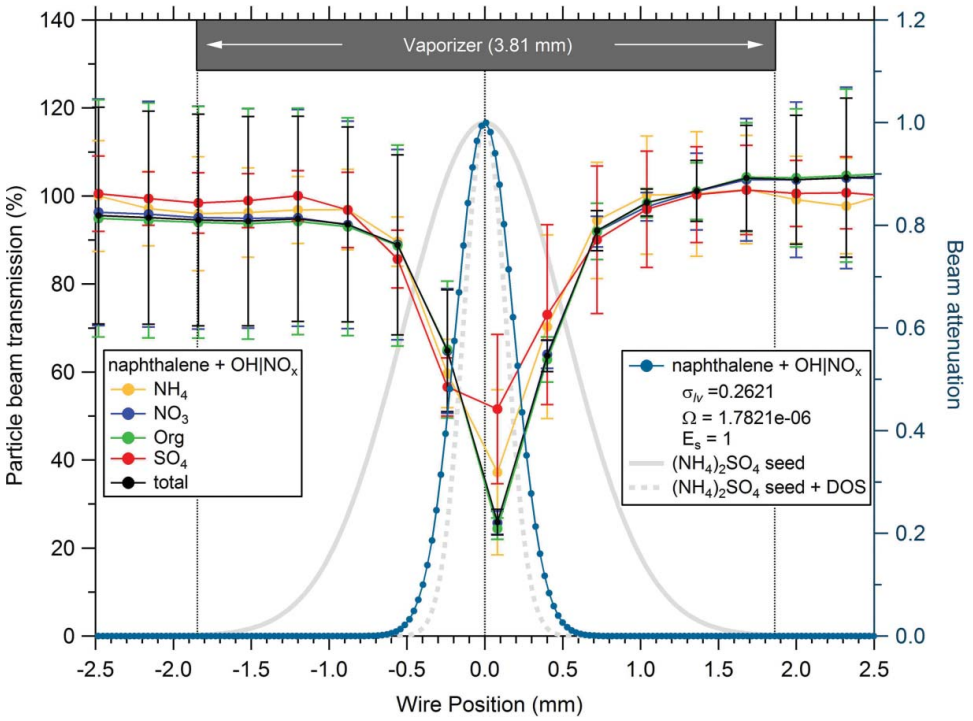

FIG. 5. Physical dimensions of the particle beam for aerosol formed from the reaction of naphthalene with the hydroxyl radical (associated with a CE/E_L~0.18) along with those of AS and DOS-coated AS particles. Beam width parameters, σ_{lv} and Ω, are calculated from beam width probe data and indicate the width of the particle beam at the vaporizer surface (in mm) and the solid angle of the particle beam (in steradians). E_S was calculated as the ratio of $\Omega_{vaporizer}/\Omega$, where $\Omega_{vaporizer} = 9.3 \times 10^{-5}$ (Huffman et al. 2005). (Color figure available online.)

a cluster of low CE values from dry reactions and another of relatively higher CE values at higher RH which we do not. As expected based on the high OM fraction, its relatively low hygroscopicity, and the relatively low RH in the chamber, CE of chamber-generated SOA is fairly insensitive to the RH of the AMS sampling line assuming that it is closely approximated by chamber RH.

Similarly, the dependence of estimated CE values on either the acidic sulfate content of or the mass fraction of AN in the particle should also be negligible due to their unlikely presence in SOA formed from these reactions. Fully neutralized AS was used as an inorganic seed particle and, although the role of acidified seed particles has been investigated in this chamber (Surratt et al. 2007a,b), none of the reactions considered here used an acidified seed. One avenue for the acid production in a subset of these reactions, however, is the formation of nitric acid (HNO_3) through the reaction of NO_x with water vapor. HNO_3, however, is likely to remain in the gas-phase and should not significantly contribute to particle acidity. Although gas phase HNO_3 can react with gas phase ammonia (NH_3) forming AN, which can influence the CE of laboratory-generated and ambient particles at high relative fractions (Matthew et al. 2008; Middlebrook et al. 2012), NH_3 chamber concentrations should be negligible making the formation of AN unlikely.

Large contributions at *m/z* 30 and 46 were observed in select reactions and should be dominated by contributions from organic nitrates (Farmer et al. 2010) and OA (e.g., CH_2O^+ at *m/z* 30). Although the unit-mass resolution of the Q-AMS used in these experiments does not allow for the separation of the nitrate and OA contributions at *m/z* 30 and *m/z* 46, the analysis of high-resolution AMS spectra from similar reactions conducted later in the same chamber indicate that the ratio of NO^+:CH_2O^+ signals at *m/z* 30 is ≥3:1 for OH/NO_x or N_2O_5 reactions (comprising nearly two-thirds of the reactions conducted here). This ratio was 1:3 for reactions conducted in the absence of NO_x where NO^+ likely arises from chamber background. As a result, the summed contribution of *m/z* 30 and *m/z* 46 to total OA (i.e., f_{NO3}) should reflect the fractional contribution of organic nitrates to OA in all experiments other than those conducted in the absence of NO_x or ozonolysis reactions. Obtained CE values are compared with the relative contributions of sulfate (f_{SO4}) and nitrate (f_{NO3}) to NR-PM_1 mass in Figures S4b and c, respectively. Overall, CE shows virtually no correlation with either f_{SO4} ($r^2 = 0.02$) or f_{NO3} ($r^2 \ll 0.01$) of each SOA type.

After discounting the role of sampling line RH and the mass fraction of acidified sulfate and AN in the aerosol, we are left to consider only the influence of the phase of the organic material on the CE of chamber-generated SOA. In their study, Matthew et al. (2008) observed that the CE of solid AS particles was increased by the presence of a layer of liquid organics (DOS), presumably through the liquid organic layer imparting to the solid particle a decreased tendency to bounce from the vaporizer

surface. For example, CE values of ~25% were obtained for dry AS particles and increased proportionally to the thickness of the DOS layer. CE = 1 was obtained for a DOS layer thickness of ~60 nm, which corresponds to a liquid organic mass fraction of ~50%. In addition to confirming the importance of particle bounce to the CE of laboratory-generated aerosols, these observations also suggest that the CE obtained for a particular SOA type may provide some broad insight into the liquid organic content of chamber-generated SOA when other factors influencing particle bounce are eliminated: low CE values on the order of ~20% imply the absence of a substantial liquid organic mass fraction while CE values near unity imply the opposite. It is more difficult to speculate as to the liquid organic mass fraction of particles with intermediate CE values other than to say that such values likely represent particles having a mixture of both solid and liquid material, or perhaps a greater fraction of higher volatility or intermediate viscosity OA material.

CE values obtained in this study for SOA produced from different reaction systems combined with the observations of Bahreini et al. (2005) confirm that not all chamber-generated SOA types are liquid inside the AMS. Indeed, CE values obtained for most reactions conducted here are considerably lower than unity indicating that, for the most part, they are solid and not liquid. It is unclear whether this equates to phase prior to their introduction into the AMS as particles are exposed to a rapidly decreasing pressure and temperature regime as they enter the vacuum system through a critical orifice, with the temperature quickly recovering. This rapid expansion into vacuum could cool the particles enough to trigger a phase transition from liquid to solid. Some recent experimental work has shown, however, that freshly nucleated chamber-generated and ambient particles can exist in a solid phase (Virtanen et al. 2010, 2011; Cappa and Wilson 2011). If this were the case, any potential supersonic cooling as the particles transition from the lens system to the vacuum chamber would be inconsequential as the particles would already be solid.

Despite the apparent causal relationship between particle phase and AMS CE for chamber-generated SOA, the question remains: what aspect of SOA composition is responsible for influencing both particle phase within the AMS and resulting CE? As discussed above and shown in Figure S4c, the contribution of what is likely to be organic nitrates appears to have a minimal influence on CE by itself. This is reasonable considering the variability in CE for SOA formed from reactions with negligible nitrate contributions and points to the existence of a more fundamental aspect of SOA composition having a primary role in determining CE.

Based on its response to AN and AS, it appears that bounce from the AMS vaporizer may be an interplay between both particle phase and volatility of the bulk material. For example, although AN and AS are both ionic solids, the volatility of AN is high enough that particles volatilize completely upon impact resulting in a CE of unity. The CE of low volatility AS, in contrast, is substantially lower until either sufficient liquid water, liquid organic, or high volatility AN is present at which point the CE gradually increases to unity. Unlike ionic salts such as AN that can be solid while still having a relatively high volatility, solid organic particles are more likely to be comprised of material having a low volatility, which is likely to be highly oxidized in the case of SOA.

Specific volatility measurements are not available for the reactions conducted in the current study. However, we can infer the volatility of the bulk SOA based on the extent of OA oxidation. Oxidation either in the atmosphere or laboratory chambers increases the functionality of the parent hydrocarbon through the addition of oxygen which increases the polarity and decreases the relative volatility of reaction products (Pandis et al. 1992). In the case of both ambient (Huffman et al. 2009b) and source specific (Huffman et al. 2009a) OA types, it has been empirically shown that increases in the degree of OA oxidation (measured as the oxygen-to-carbon molecular ratio, O:C) are associated with corresponding decreases in volatility. This relationship between O:C and volatility has recently been used to model the aging of OA in the atmosphere (Jimenez et al. 2009; Donahue et al. 2012), which proposes that the volatility and O:C ratio of OA components are inversely proportional as OA ages in the atmosphere. Because the volatility of SOA generated in these reactions should be dictated by the organic fraction due to its overwhelming (>95%) contribution to particle mass, a low O:C would suggest relatively higher volatility while a higher O:C suggests the opposite.

The O:C ratio of organic aerosols can be measured using high-resolution AMS mass spectra or, in cases where only unit mass resolution AMS spectra are available, estimated using the ratio of *m/z* 44 (which is comprised almost entirely of CO_2^+ in AMS spectra) to the total AMS organic signal (f_{44}) (Aiken et al. 2008). Based on the empirical relationship between phase and volatility in the case of OA, where relatively low volatilities are required to form solid OA, we can explore the potential role of phase on particle bounce using f_{44} as a surrogate for bulk volatility. Adjusted CE values (i.e., CE/($E_L \times E_S$)) are used to approximate E_B and are plotted versus corresponding f_{44} values in Figure S4d. Although adjusted CE and f_{44} values have a low degree of correlation ($r^2 = 0.34$), the data reveal a trend wherein low f_{44} values correspond to a high adjusted CE while high f_{44} values correspond to a low adjusted CE. Based on the low degree of correlation observed between these two metrics, it appears that higher O:C (and the correlated lower particle volatility) may increase the likelihood that a particle will bounce from the vaporizer, but by itself does not fully account for the variability in observed E_B values.

In contrast to *m/z* 44, which is a prominent fragment in AMS mass spectra of highly oxidized OA, *m/z* 57 is a prominent fragment of AMS mass spectra of reduced hydrocarbons, including petroleum sources such as fuel and oil, and has been used as a marker for primary combustion emissions in AMS spectra (Zhang et al. 2005). The majority of signal at *m/z* 57 is contributed by both reduced ($C_4H_9^+$) and oxidized ($C_3H_5O^+$) ions. While $C_4H_9^+$ likely dominates the composition of *m/z* 57 in ambient OA due to the presence of directly emitted

reduced hydrocarbons, $C_3H_5O^+$ likely should have larger contributions in chamber-generated SOA mass spectra. Indeed, we observe a $C_3H_5O^+$:$C_4H_9^+$ ratio of 3:1 in high-resolution mass spectra of SOA formed in reactions conducted in our chamber similar to those discussed here. Reduced and less oxidized hydrocarbons have a higher volatility relative to highly oxidized organic aerosols (Huffman et al. 2009b) and nonoxygen containing ions in the spectra of chamber-generated SOA arise from more volatile species than those producing CO_2^+ (Huffman et al. 2009a). It would be reasonable to expect, therefore, that larger contributions from reduced or less oxidized fragments such as $C_4H_9^+$ or $C_3H_5O^+$, respectively, to the total AMS organic signal would correlate with a higher volatility of the corresponding SOA. Comparing adjusted CE values against the corresponding ratio of *m/z* 57 to total AMS organic signal (f_{57}) appears to show that this is the case as shown in Figure S4e. Overall, the trend between the adjusted CE and f_{57} is generally opposite that observed between adjusted CE and f_{44} (e.g., low f_{57} are associated with low E_B and visa versa) and has a similarly low degree of correlation ($r^2 = 0.32$). Adjusted CE values are also plotted against the relative contribution of *m/z* 43 to AMS organic signal (i.e., f_{43}) in Figure S4f, which displays a trend similar to but with much lower correlation than that between CE and f_{44}. This is different from the relationship between adjusted CE and *m/z* 57 and is likely due to the higher contribution of oxidized ($C_2H_3O^+$) relative to reduced ($C_3H_7^+$) ions in the case of *m/z* 43. This has been noted for ambient OA (Ng et al. 2010) and is consistent with a $C_2H_3O^+$:$C_3H_7^+$ ratio of ~10:1 in high-resolution mass spectra of SOA formed in reactions in our chamber similar to those discussed here. Overall, these observations indicate that *m/z* 57 has a higher average volatility than *m/z* 43 due to the higher relative contribution from reduced ions.

It is important to note that we are using surrogates for bulk composition and volatility (i.e., f_{44} and f_{57}) in order to make general inferences about the phase of various SOA types and its influence on obtained CE values. We believe that these inferences are reasonable based on the relationship between OA oxidation and bulk volatility and previous empirical results demonstrating the importance of phase, and particularly solid particles, to low CE values when sampling with the AMS. However, determining with certainty the relationship between volatility and phase and the resulting impact of particle bounce on CE values would require additional measurements of volatility which are not available here.

Interestingly, a substantially larger fraction of the variability in particle bounce appears to be explained by the ratio of the relative contribution of f_{44} to f_{57} (i.e., f_{44}/f_{57}). Adjusted CE values are plotted versus f_{44}/f_{57} in Figure 6a along with a sigmoidal fit. Note that f_{44}/f_{57} is shown on a log scale in Figures 6a and b

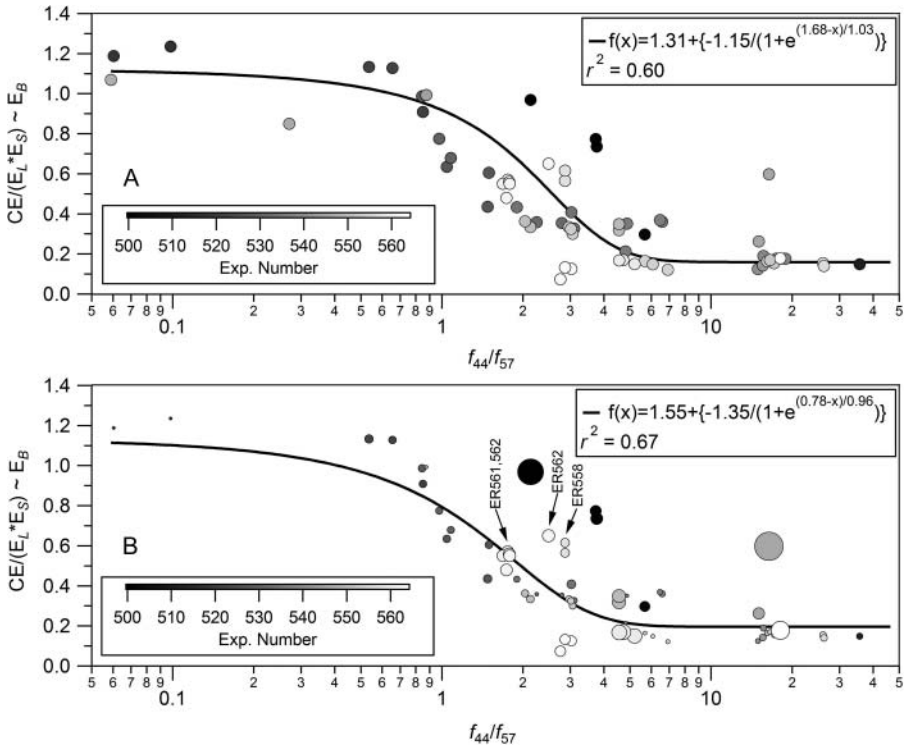

FIG. 6. Estimated E_B values as a function of the f_{44}/f_{57} ratio. Data in (a) are shown without correcting for the overestimated E_L contribution to ER588, ER561, and ER562. This overestimation has been removed from the data presented in (b) (indicated by arrows), which has decreased the CE for each of these reactions to a point where they are much more consistent with the majority of remaining aerosols. A sigmoid regression curve has been added to each plot to show the overall data trend. Additionally, marker size in (b) indicates the relative contribution of nitrate to OA mass (f_{NO3}, range: 0–40%) for each aerosol type.

for clarity. As Figure 6a shows, when $f_{44} \ll f_{57}$, adjusted CE values are essentially unity within the combined error of each measurement indicating a low incidence of particle bounce. CE values continue to be unity until $f_{44} \sim f_{57}$ at which point CE steadily declines to an average minimum of ~20% for $f_{44} \gg f_{57}$. The correlation between adjusted CE and $\log(f_{44}/f_{57})$ is relatively high ($r^2 = 0.60$) compared to that between adjusted CE and either f_{44} or f_{57}. Despite this correlation, there are a few outliers in the middle of the f_{44}/f_{57} range that lie above the trend line.

Many of these outlying data points are associated with those experiments for which the AMS mass distribution is substantially larger than the lens transmission curve, potentially leading to an underestimated E_L values and an overestimated E_B contribution as discussed above (Figure S3). If we calculate E_L for these reactions using the linear regression results shown in Figure 4, the adjusted CE values decrease as shown in Figure 6b (adjusted values are indicated by arrows). This slight correction brings CE values for these reactions much closer to the trend line and increases the correlation ($r^2 = 0.67$) between adjusted CE and $\log(f_{44}/f_{57})$ relative to the uncorrected case shown in Figure 6a. Additionally, the size of data points in Figure 6b reflects the relative contribution of presumably organic nitrate to NR-PM_1 (i.e., larger symbols represent larger nitrate fractions). Many of the remaining outlying data points remaining in Figure 6b are associated with large relative contributions from nitrate suggesting that the contribution of organic nitrate may have a secondary impact in reducing particle bounce. However, this trend is obscured by the presence of several SOA types with equally large nitrate fractions where CE is reasonably predicted by the trend line indicating that the role of the nitrate fraction of SOA may be considerably more complicated.

To our knowledge, these results are the first to indicate a role of OA composition on the CE of the AMS when sampling either laboratory or ambient particles dominated by SOA. However, they appear to be consistent with those of Saukko et al. (2012) who recently reported on humidity-dependent phase states of SOA from oxidation of biogenic and anthropogenic sources by measuring particle bounce behavior after inertial impaction. In addition to a decrease in the fraction of particles that bounce from the impaction surface as a result of prolonged exposure to high RH, results of this study also showed that the bounce fraction substantially increased with increasing degree of organic oxidation. As is the case here, however, the bounce behavior of the various SOA types was not highly correlated with the corresponding O/C of the particle indicating a more complex dependency of particle phase and the bounce behavior on additional factors.

We recommend that the OA composition dependency of CE be applied when generating quantitative results for chamber-generated SOA. Caution should be exercised, however, when this correction is applied to SOA formed from reactions outside the scope of those performed here, and we recommend that a quantification of CE similar to that carried out here be performed by researchers in other chambers. It is less clear whether our results for chamber SOA are applicable to ambient OA or the various types of POA, some of which can have high O:C (Huffman et al. 2009a). For example, we are unaware of CE values below ~50% for ambient OA and Middlebrook et al. (2012) observed CE~50% for organic-dominated particles in two separate studies incorporating ambient measurements from a variety of locations. A disparity also exists between the CE of AS in laboratory and ambient settings. The CE of pure dry laboratory AS particles is ~20–25% (Matthew et al. 2008), while that of ambient particles is ~50% based on comparison of AMS and comparable sulfate measurements. This could be due to the more complex nature of ambient particles resulting in particle phases with a lower tendency to bounce than pure laboratory SOA of high O:C, or than AS particles. For this reason, the possible influence of f_{44}/f_{57} on CE of ambient organics and its potential to improve the agreement between AMS and collocated OA measurements should be the focus of future research. It is important that these and other future studies investigating AMS CE be conducted with a minimum of two independent measurements as was done here in order to avoid improperly attributing potential measurement artifacts to AMS CE.

4. CONCLUSIONS

The CE of the AMS for chamber-generated SOA was investigated by comparing the responses of the AMS to that of an SMPS, Sunset semi-continuous OC monitor, and gravimetric filter measurements. CE values were highly variable ranging from unity to an average minimum of 20%, which is similar to the CE for dry, solid AS particles. Similar to previous investigations on the CE of ambient and laboratory-generated particles, mass losses due to particles impacting interior surfaces of the AMS aerodynamic lens system and due to beam broadening in the time-of-flight chamber are minimal and most of the discrepancy between mass measured by the AMS and other techniques is due to bounce of particles from the vaporizer surface prior to volatilization. Conditions that have previously been determined to impact particle bounce including the RH of the sampling line, the particle mass fraction of AN, and the contribution of acidic sulfate are very unlikely to cause the behavior observed here. The presence of liquid-phase or high-volatility organics in or surrounding the particle, on the other hand, may have a dominant influence on CE of chamber-generated SOA. The bounce of chamber-generated SOA was most strongly correlated with the ratio of f_{44}/f_{57}: CE values near unity are observed for SOA with $f_{44} \ll f_{57}$ and decrease to an average minimum of approximately 20% are observed for SOA with $f_{44} \gg f_{57}$. The relative contribution of organic nitrates might also play a subordinate role in determining CE values. These observations strongly suggest that SOA composition plays a large role in determining the phase and CE of chamber generated SOA. Additional study is required to understand whether and how SOA composition (in particular the f_{44}/f_{57} ratio) determines liquid organic content

and whether particle phase determined by the AMS is representative of these same particles prior to their introduction to the AMS. It is unclear whether these results are applicable to mixed ambient particles, for which CE values below ∼0.5 have not been reported, and this should be the subject of future research.

REFERENCES

Aiken, A. C., Decarlo, P. F., Kroll, J. H., Worsnop, D. R., Huffman, J. A., Docherty, K. S., et al. (2008). O/C and OM/OC Ratios of Primary, Secondary, and Ambient Organic Aerosols with High-Resolution Time-of-Flight Aerosol Mass Spectrometry. *Environ. Sci. Technol.*, 42(12):4478–4485.

Aiken, A. C., Salcedo, D., Cubison, M. J., Huffman, J. A., DeCarlo, P. F., Ulbrich, I. M., et al. (2009). Mexico City Aerosol Analysis During MILAGRO Using High Resolution Aerosol Mass Spectrometry at the Urban Supersite (T0) - Part 1: Fine Particle Composition and Organic Source Apportionment. *Atmos. Chem. Phys.,* 9(17):6633–6653.

Alfarra, M. R. (2004). Insights Into Atmospheric Organic Aerosols Using an Aerosol Mass Spectrometer. Ph.D. thesis, University of Manchester, Manchester, UK.

Allan, J. D., Alfarra, M. R., Bower, K. N., Williams, P. I., Gallagher, M. W., Jimenez, J. L., et al. (2003). Quantitative Sampling Using an Aerodyne Aerosol Mass Spectrometer 2. Measurements of Fine Particulate Chemical Composition in Two U.K. Cities. *J. Geophys. Res.,* 108(D3):4091, doi:10.1029/2002JD002359.

Allan, J. D., Delia, A. E., Coe, H., Bower, K. N., Alfarra, M. R., Jimenez, J. L., et al. (2004). A Generalised Method for the Extraction of Chemically Resolved Mass Spectra From Aerodyne Aerosol Mass Spectrometer Data. *J. Aerosol. Sci.,* 35(7):909–922.

Bahreini, R., Dunlea, E. J., Matthew, B. M., Simons, C., Docherty, K. S., DeCarlo, P. F., et al. (2008). Design and Operation of a Pressure-Controlled Inlet for Airborne Sampling with an Aerodynamic Aerosol Lens. *Aerosol Sci. Technol.,* 42(6):465–471.

Bahreini, R., Keywood, M. D., Ng, N. L., Varutbangkul, V., Gao, S., Flagan, R. C., et al. (2005). Measurements of Secondary Organic Aerosol (SOA) from Oxidation of Cycloalkenes, Terpenes, and *m*-xylene Using an Aerodyne Aerosol Mass Spectrometer. *Aerosol Sci. Technol.*, 39(15):5674–5688.

Canagaratna, M., Jayne, J., Jimenez, J., Allan, J., Alfarra, M., Zhang, Q., et al. (2007). Chemical and Microphysical Characterization of Ambient Aerosols with the Aerodyne Aerosol Mass Spectrometer. *Mass Spec. Rev.,* 26(2):185–222.

Cappa, C. D., and Wilson, K. R. (2011). Evolution of Organic Aerosol Mass Spectra Upon Heating: Implications for OA Phase and Partitioning Behavior. *Atmos. Chem. Phys.,* 11(5):1895–1911.

Chhabra, P. S., Flagan, R. C., and Seinfeld, J. H. (2010). Elemental Analysis of Chamber Organic Aerosol Using an Aerodyne High-Resolution Aerosol Mass Spectrometer. *Atmos. Chem. Phys.,* 10(9):4111–4131.

Cross, E. S., Onasch, T. B., Canagaratna, M., Jayne, J. T., Kimmel, J., Yu, X. Y., et al. (2009). Single Particle Characterization Using a Light Scattering Module Coupled to a Time-of-Flight Aerosol Mass Spectrometer. *Atmos. Chem. Phys.,* 9(20):7769–7793.

DeCarlo, P. F., Kimmel, J. R., Trimborn, A., Northway, M. J., Jayne, J. T., Aiken, A. C., et a. (2006). Field-Deployable, High-Resolution, Time-of-Flight Aerosol Mass Spectrometer. *Anal. Chem.*, 78(24):8281–8289.

DeCarlo, P. F., Slowik, J. G., Worsnop, D. R., Davidovits, P., and Jimenez, J. L. (2004). Particle Morphology and Density Characterization by Combined Mobility and Aerodynamic Diameter Measurements. Part 1: Theory. *Aerosol Sci. Technol.,* 38(12):1185–1205.

Delia, A. E. (2004). Real-Time Measurements of Non-Refractory Particle Composition and Interactions at Forested Sites. Ph.D. thesis, University of Colorado, Colorado.

Docherty, K. S., Aiken, A. C., Huffman, J. A., Ulbrich, I. M., DeCarlo, P. F., Sueper, D., et al. (2011). The 2005 Study of Organic Aerosols at Riverside (SOAR-1): Instrumental Intercomparisons and Fine Particle Composition. *Atmos. Chem. Phys.,* 11(23):12387–12420.

Donahue, N. M., Kroll, J. H., Pandis, S. N., and Robinson, A. L. (2012). A Two-Dimensional Volatility Basis Set - Part 2: Diagnostics of Organic-Aerosol Evolution. *Atmos. Chem. Phys.,* 12:615–634.

Duplissy, J., DeCarlo, P. F., Dommen, J., Alfarra, M. R., Metzger, A., Barmpadimos, I., et al. (2011). Relating Hygroscopicity and Composition of Organic Aerosol Particulate Matter. *Atmos. Chem. Phys.,* 11(3):1155–1165.

Edney, E. O., Kleindienst, T. E., Jaoui, M., Lewandowski, M., Offenberg, J. H., Wang, W., et al. (2005). Formation of 2-Methyl Tetrols and 2-Methylglyceric Acid in Secondary Organic Aerosol From Laboratory Irradiated Isoprene/NO(X)/SO(2)/Air Mixtures and Their Detection in Ambient PM(2.5) Samples Collected in the Eastern United States. *Atmos. Environ.,* 39(29):5281–5289.

Engelhart, G. J., Asa-Awuku, A., Nenes, A., and Pandis, S. N. (2008). CCN Activity and Droplet Growth Kinetics of Fresh and Aged Monoterpene Secondary Organic Aerosol. *Atmos. Chem. Phys.,* 8(14):3937–3949.

Farmer, D. K., Matsunaga, A., Docherty, K. S., Surratt, J. D., Seinfeld, J. H., Ziemann, P. J., et al. (2010). Response of an Aerosol Mass Spectrometer to Organonitrates and Organosulfates and Implications for Atmospheric Chemistry. *Proc. Natl. Acad. Sci. USA,* 107(15):6670–6675.

Hinds, W. C. (1999). *Aerosol Technology*. Wiley Interscience, New York.

Huffman, J. A., Docherty, K. S., Aiken, A. C., Cubison, M. J., Ulbrich, I. M., DeCarlo, P. F., et al. (2009b). Chemically-Resolved Aerosol Volatility Measurements from Two Megacity Field Studies. *Atmos. Chem. Phys.,* 9(18):7161–7182.

Huffman, J. A., Docherty, K. S., Mohr, C., Cubison, M. J., Ulbrich, I. M., Ziemann, P. J., et al. (2009a). Chemically-Resolved Volatility Measurements of Organic Aerosol from Different Sources. *Environ. Sci. Technol.,* 43(14):5351–5357.

Huffman, J. A., Jayne, J. T., Drewnick, F., Aiken, A. C., Onasch, T., Worsnop, D. R., et al. (2005). Design, Modeling, Optimization, and Experimental Tests of a Particle Beam Width Probe for the Aerodyne Aerosol Mass Spectrometer. *Aerosol Sci. Technol.,* 39(12):1143–1163.

Jayne, J. T., Leard, D. C., Zhang, Z., Davidovits, P., Smith, K. A., Kolb, C. E., et al. (2000). Development of an Aerosol Mass Spectrometer for Size and Composition Analysis of Submicron Particles. *Aerosol Sci. Technol.,* 33:49–70.

Jimenez, J. L., Canagaratna, M. R., Donahue, N. M., Prevot, A. S. H., Zhang, Q., Kroll, J. H., et al. (2009). Evolution of Organic Aerosols in the Atmosphere. *Science,* 326(5959):1525–1529.

Jimenez, J. L., Jayne, J. T., Shi, Q., Kolb, C. E., Worsnop, D. R., Yourshaw, I., et al. (2003). Ambient Aerosol Sampling Using the Aerodyne Aerosol Mass Spectrometer. *J. Geophys. Res.-Atmos.,* 108(D7):8425, doi:10.1029/2001 JD001213.

Kuwata, M., Zorn, S. R., and Martin, S. T. (2012). Using Elemental Ratios to Predict the Density of Organic Material Composed of Carbon, Hydrogen, and Oxygen. *Environ. Sci. Technol.,* 46(2):787–794.

Liu, P. S. K., Deng, R., Smith, K. A., Williams, L. R., Jayne, J. T., Canagaratna, M. R., et al. (2007). Transmission Efficiency of an Aerodynamic Focusing Lens System: Comparison of Model Calculations and Laboratory Measurements for the Aerodyne Aerosol Mass Spectrometer. *Aerosol Sci. Technol.,* 41(8):721–733.

Matthew, B. M., Middlebrook, A. M., and Onasch, T. B. (2008). Collection Efficiencies in an Aerodyne Aerosol Mass Spectrometer as a Function of Particle Phase for Laboratory Generated Aerosols. *Aerosol Sci. Technol.,* 42(11):884–898.

McMurry, P. H. (2000). A Review of Atmospheric Aerosol Measurements. *Atmos. Environ.,* 34(12–14):1959–1999.

Middlebrook, A. M., Bahreini, R., Jimenez, J. L., and Canagaratna, M. R. (2012). Evaluation of Composition-Dependent Collection Efficiencies for the Aerodyne Aerosol Mass Spectrometer using Field Data. *Aerosol Sci. Technol.,* 46(3):258–271.

Ng, N.L., Canagaratna, M.R., Zhang, Q., Jimenez, J.L., Tian, J., Ulbrich, I.M., et al. (2010). Organic Aerosol Components Observed in Northern

Hemispheric Datasets from Aerosol Mass Spectrometry. *Atmos. Chem. Phys.,* 10:4625–4641.

Pandis, S. N., Harley, R. A., Cass, G. R., and Seinfeld, J. H. (1992). Secondary Organic Aerosol Formation and Transport. *Atmos. Environ. A,* 26(13):2269–2282.

Prenni, A. J., Petters, M. D., Kreidenweis, S. M., DeMott, P. J., and Ziemann, P. J. (2007). Cloud Droplet Activation of Secondary Organic Aerosol. *J. Geophys. Res.-Atmos.* 112:D10223, doi:10.1029/2006JD007963.

Quinn, P. K., Bates, T. S., Coffman, D., Onasch, T. B., Worsnop, D., Baynard, T., et al. (2006). Impacts of Sources and Aging on Submicrometer Aerosol Properties in the Marine Boundary Layer Across the Gulf of Maine. *J. Geophys. Res.-Atmos.,* 111:D23S36, doi:10.1029/2006JD007582.

Salcedo, D., Dzipina, K., Onasch, T. B., Canagaratna, M. R., Zhang, Q., Huffman, J. A., et al. (2005). Characterization of Ambient Aerosols in Mexico City During the MCMA-2003 Campaign with Aerosol Mass Spectometry - Part I: Quantification, Shape-Related Collection Efficiency, and Comparison with Collocated Instruments. *Atmos. Phys. Chem. Discuss.,* 5:4143–4182.

Salcedo, D., Onasch, T. B., Aiken, A. C., Williams, L. R., de Foy, B., Cubison, M. J., et al. (2010). Determination of Particulate Lead Using Aerosol Mass Spectrometry: MILAGRO/MCMA-2006 Observations. *Atmos. Chem. Phys.* 10:65371–5389.

Salcedo, D., Onasch, T. B., Canagaratna, M. R., Dzepina, K., Huffman, J. A., Jayne, J. T., et al. (2007). Technical Note: Use of a Beam Width Probe in an Aerosol Mass Spectrometer to Monitor Particle Collection Efficiency in the Field. *Atmos. Chem. Phys.,* 7:549–556.

Salcedo, D., Onasch, T. B., Dzepina, K., Canagaratna, M. R., Zhang, Q., Huffman, J. A., et al. (2006). Characterization of Ambient Aerosols in Mexico City During the MCMA-2003 Campaign with Aerosol Mass Spectrometry: Results from the CENICA Supersite. *Atmos. Chem. Phys.,* 6:925–946.

Saukko, E., Lambe, A. T., Massoli, P., Koop, T., Wright, J. P., Croasdale, D. R., et al. (2012). Humidity-Dependent Phase State of SOA Particles from Biogenic and Anthropogenic Precursors. *Atmos. Chem. Phys.,* 12:7517–7259.

Surratt, J. D., Kroll, J. H., Kleindienst, T. E., Edney, E. O., Claeys, M., Sorooshian, A., et al. (2007a). Evidence for Organosulfates in Secondary Organic Aerosol. *Environ. Sci. Technol.,* 41(2):517–527.

Surratt, J. D., Lewandowski, M., Offenberg, J. H., Jaoui, M., Kleindienst, T. E., Edney, E. O., et al. (2007b). Effect of Acidity on Secondary Organic Aerosol Formation from Isoprene. *Environ. Sci. Technol.,* 41(15):5363–5369.

Takegawa, N., Miyakawa, T., Watanabe, M., Kondo, Y., Miyazaki, Y., Han, S., et al. (2009). Performance of an Aerodyne Aerosol Mass Spectrometer (AMS) during Intensive Campaigns in China in the Summer of 2006. *Aerosol Sci. Technol.,* 43(3):189–204.

Turpin, B. J., and Lim, H. J. (2001). Species Contributions to PM2.5 Mass Concentrations: Revisiting Common Assumptions for Estimating Organic Mass. *Aerosol Sci. Technol.,* 35(1):602–610.

Varutbangkul, V., Brechtel, F. J., Bahreini, R., Ng, N. L., Keywood, M. D., Kroll, J. H., et al. (2006). Hygroscopicity of Secondary Organic Aerosols Formed by Oxidation of Cycloalkenes, Monoterpenes, Sesquiterpenes, and Related Compounds. *Atmos. Chem. Phys.,* 6:2367–2388.

Virtanen, A., Joutsensaari, J., Koop, T., Kannosto, J., Yli-Pirila, P., Leskinen, J., et al. (2010). An Amorphous Solid State of Biogenic Secondary Organic Aerosol Particles. *Nature,* 467(7317):824–827.

Virtanen, A., Kannosto, J., Kuuluvainen, H., Arffman, A., Joutsensaari, J., Saukko, E., et al. (2011). Bounce Behavior of Freshly Nucleated Biogenic Secondary Organic Aerosol Particles. *Atmos. Chem. Phys.,* 11(16):8759–8766.

Weimer, S., Drewnick, F., Hogrefe, O., Schwab, J. J., Rhoads, K., Orsini, D., et al. (2006). Size-Selective Nonrefractory Ambient Aerosol Measurements During the Particulate Matter Technology Assessment and Characterization Study - New York 2004 Winter Intensive in New York City. *J. Geophys. Res.-Atmos.,* 111:D18305, doi:10.1029/2006JD007215.

Zelenyuk, A., Imre, D., and Cuadra-Rodriguez, L. A. (2006). Evaporation of Water from Particles in the Aerodynamic Lens Inlet: An Experimental Study. *Anal. Chem.* 78(19):6942–6947.

Zhang, Q., Worsnop, D. R., Canagaratna, M. R., and Jimenez, J. L. (2005). Hydrocarbon-Like and Oxygenated Organic Aerosols in Pittsburgh: Insights Into Sources and Processes of Organic Aerosols. *Atmos. Chem. Phys.,* 5:3289–3311.

Zhang, X. F., Smith, K. A., Worsnop, D. R., Jimenez, J. L., Jayne, J. T., Kolb, C. E., et al. (2004). Numerical Characterization of Particle Beam Collimation: Part II - Integrated Aerodynamic-Lens-Nozzle System. *Aerosol Sci. Technol.,* 38(6):619–638.

Supplemental Information for Collection Efficiency of the Aerosol Mass Spectrometer for Chamber-Generated Secondary Organic Aerosols

Kenneth S. Docherty[1,*], Mohammed Jaoui[1], Eric Corse[1], Jose L. Jimenez[2], John H. Offenberg[3], Michael Lewandowski[3], Tadeusz E. Kleindienst[3]

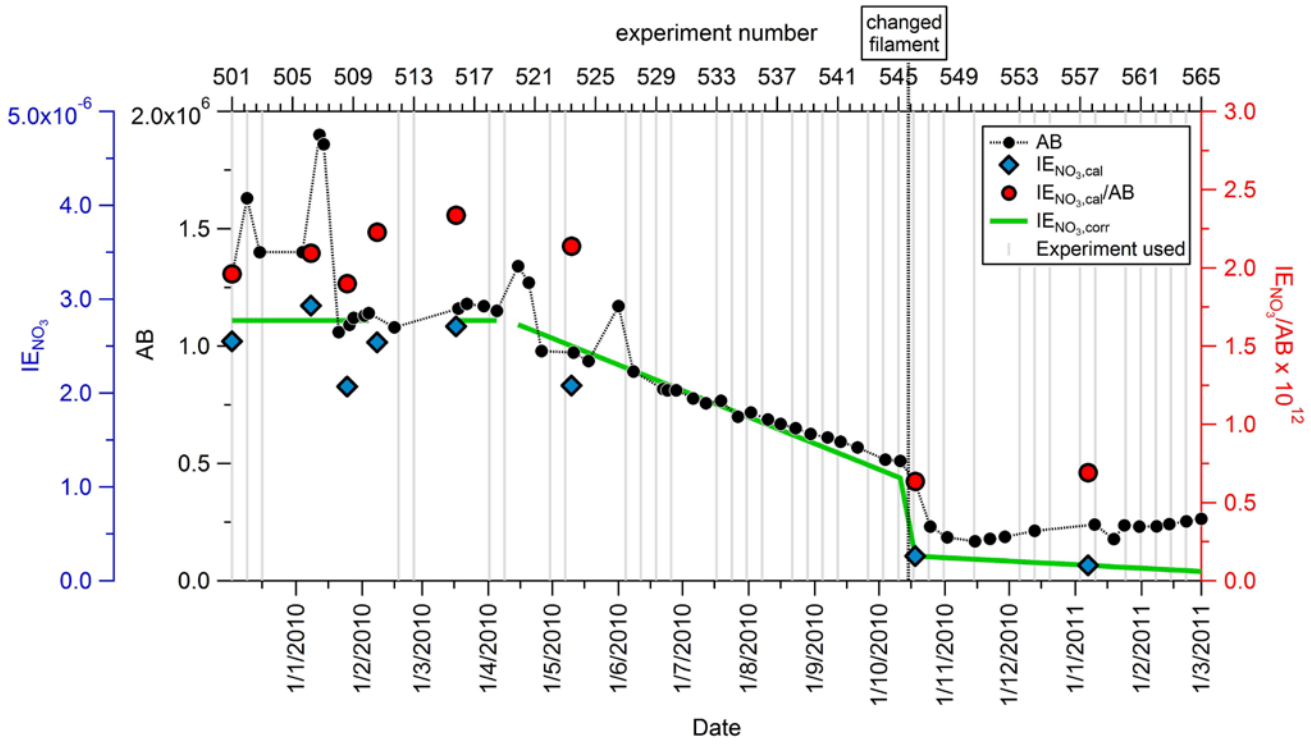

Figure S1. Q-AMS ionization efficiency (IE) calibration data. The ionization efficiency of the AMS was calibrated periodically with ammonium nitrate throughout the range of experiments considered herein. Shown here are the instrument air beam (AB) measured during each experiment, individual calibration values including IE ($IE_{NO3,cal}$) and IE/AB ($IE_{NO3,cal}/AB$) ratios, and IE values used during data analysis ($IE_{NO3,corr}$).

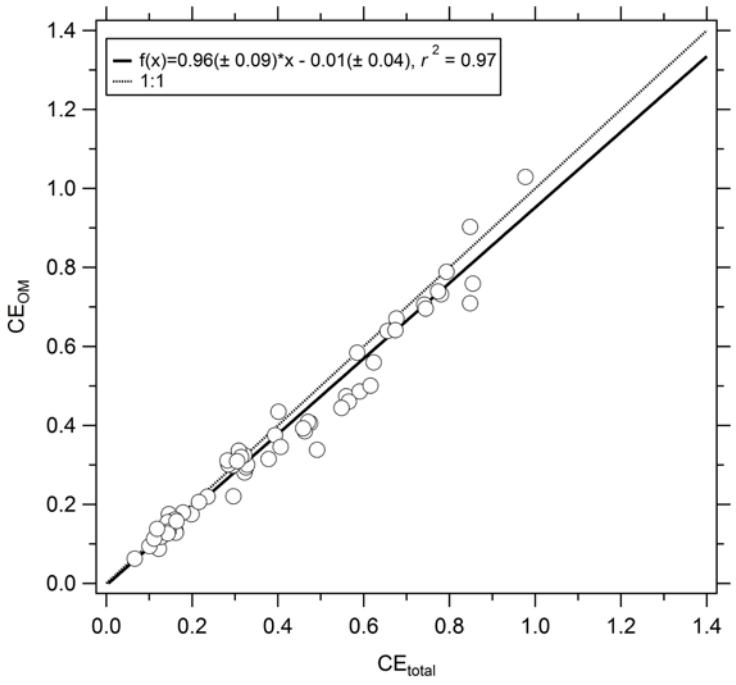

Figure S2. Comparison of calculated CE_{OM} and CE_{total} values for the range of experiments investigated in this study. As expected based on the dominant contribution of OA in aerosol formed in each of the experiments, CE_{OM} and CE_{total} values are consistent and highly correlated indicating a negligible role for ammonium sulfate seed aerosols.

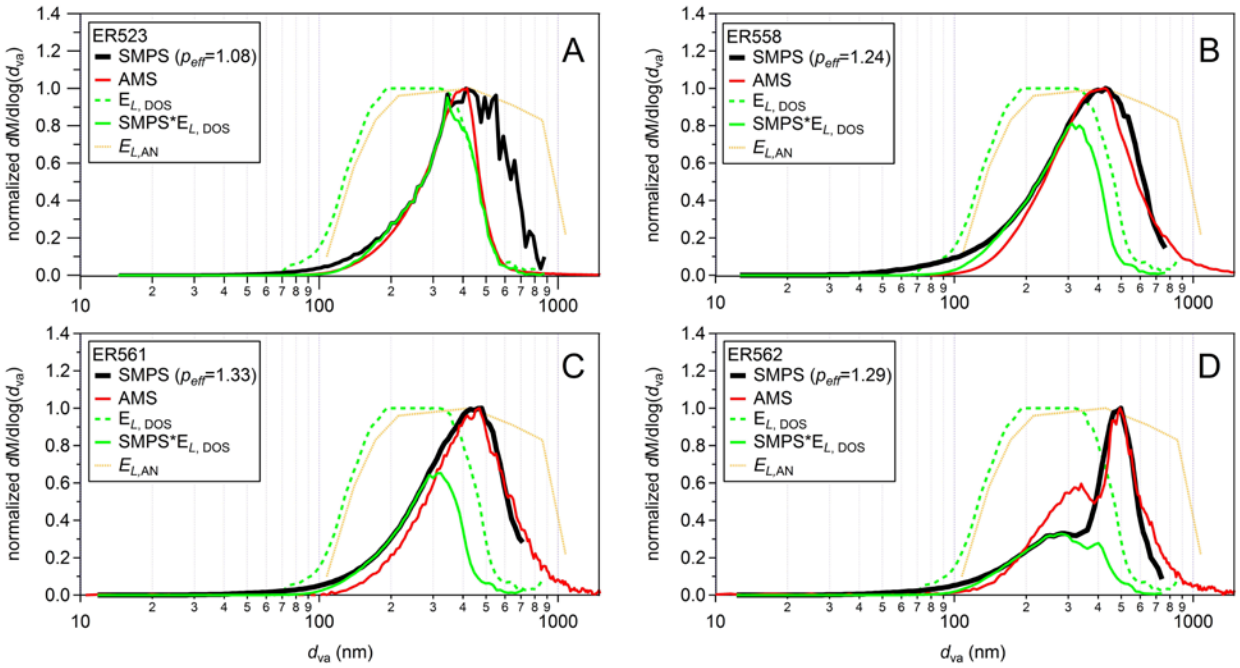

Figure S3. SMPS and AMS particle size distributions from reactions ER523 (A), ER558 (B), ER561 (C), and ER562 (D). In each case, SMPS mass distributions have been shifted by p_{eff} to match AMS distributions. $E_{L,DOS}$ and adjusted SMPS distributions (i.e., SMPS* $E_{L,DOS}$) are also shown to clearly display both the transmission efficiency of the AMS aerodynamic lens system and the estimated contribution of $E_{L,DOS}$ to CE. Unlike those from other experiments conducted in this study, particle size distributions from these experiments extend outside the optimum size range for the AMS lens. AMS and SMPS* $E_{L,DOS}$ obtained from ER523 are consistent despite the contribution of large particles. Those obtained from ER588, ER561, and ER562 are highly different with SMPS* $E_{L,DOS}$ reporting substantially less mass than corresponding AMS distributions. The contribution of E_L to CE in these latter experiments is significantly overestimated as a result.

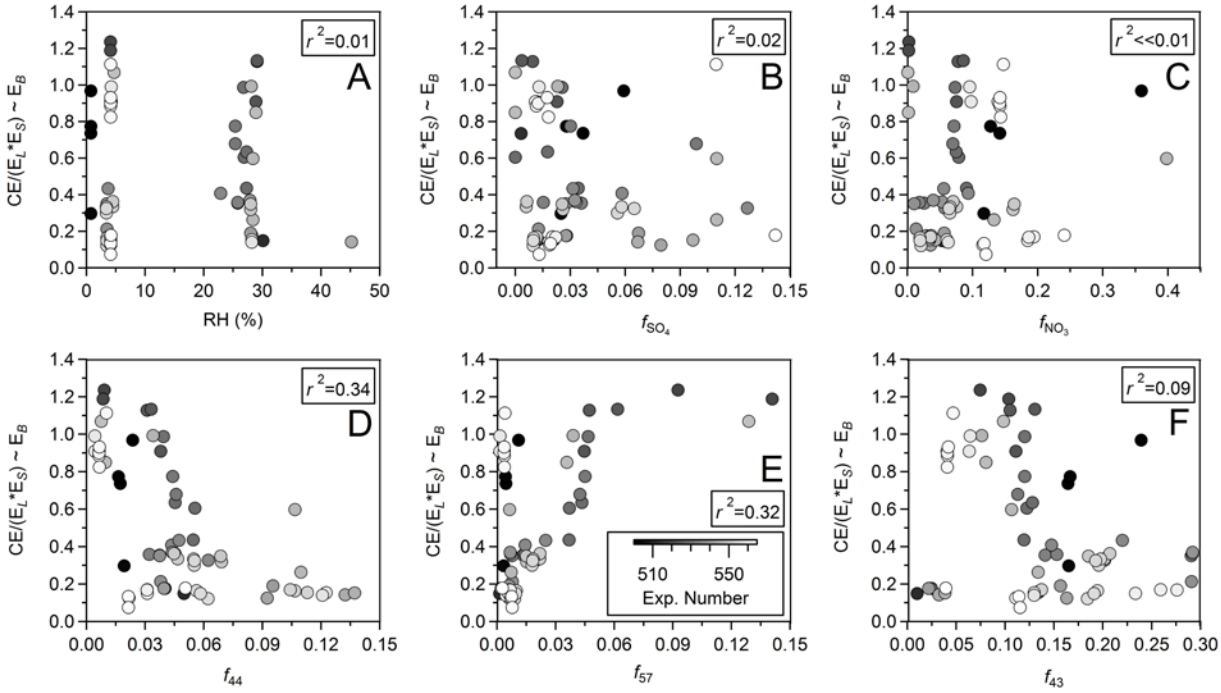

Figure S4. Scatter plots investigating the relationship between E_B and various bulk aerosol and OM parameters.

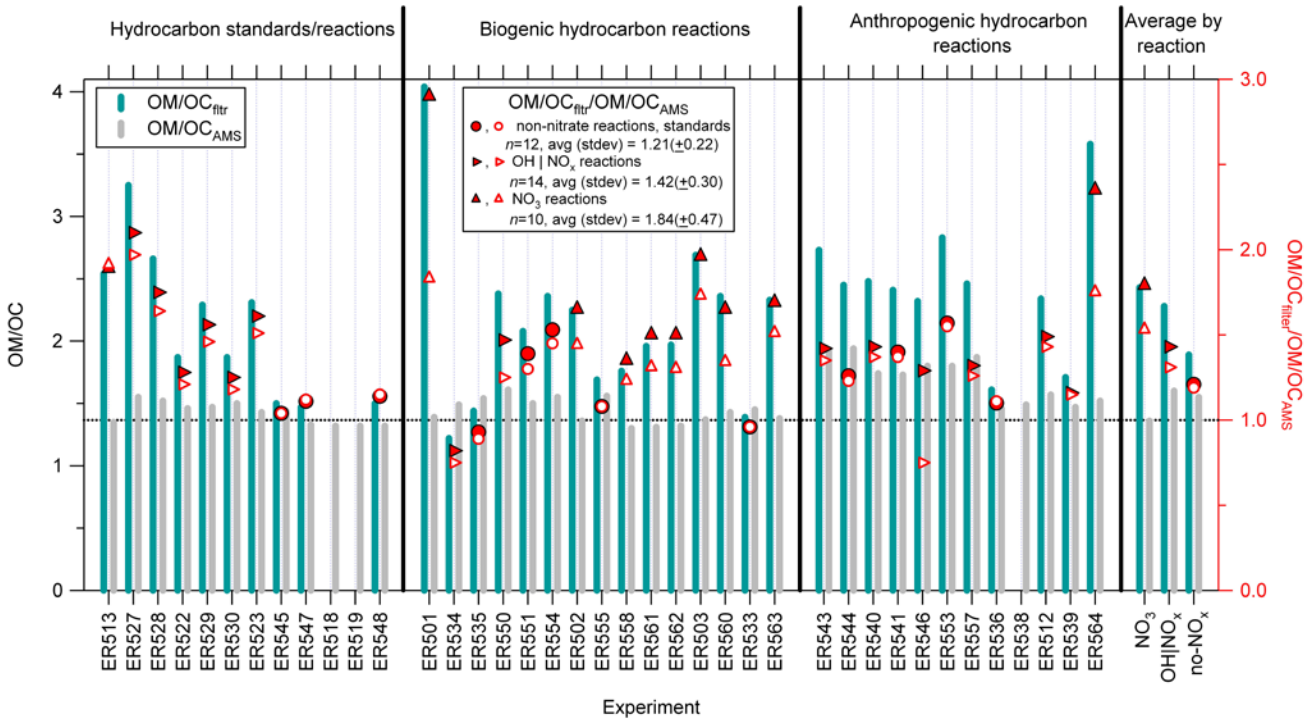

Figure S5. OM/OC values obtained from filter OM and Sunset OC measurements (OM/OC_{fltr}), along with those calculated from AMS data (OM/OC_{AMS}) and the ratio between the two ($OM/OC_{fltr}/OM/OC_{AMS}$). Overall, OM/OC_{fltr} values are higher than OM/OC_{AMS} while OM/OC_{AMS} values tend to be closer to literature and theoretical values in most cases. $OM/OC_{fltr}/OM/OC_{AMS}$ values have been divided among reaction types (i.e., non-NO_x/standards (●), OH|NO_x reactions (►), and NO_3 reactions (▲)) and two values are shown for each reaction to explore the potential for NO_2 moieties (Farmer et al., 2010) to contribute to the difference between OM/OC_{fltr} and OM/OC_{AMS} as average $OM/OC_{fltr}/OM/OC_{AMS}$ ratios are highest for those reactions where NO_2 moieties are more likely (i.e., NO_3 > OH|NO_x > non-NO_x, standards). Solid symbols represent OM/OC_{AMS} values calculated using f_{44} and its relationship to OM/OC (Aiken et al., 2008) while open symbols represent OM/OC_{AMS} values calculated with summed OM and nitrate mass concentrations. $OM/OC_{fltr}/OM/OC_{AMS}$ values decrease ~15% in the case of NO_3 reactions, ~8% for OH|NOx reactions, and remain about the same for non-NOx, standards indicating that, while NO_2 moieties can contribute to differences in OM/OC obtained from the two different methods, OM/OC_{fltr} values remain substantially higher than corresponding OM/OC_{AMS} values even when NO_2 moieties are considered. This in turn suggests that either artifacts associated with either filter OM or Sunset OC measurements, and/or other potential biases in the AMS measurement are responsible for the remaining difference.

Table S1. Experimental details

	Date	Hydrocarbon	Oxidant	Seed	$[Vol]_{Seed}$ $\mu m^3\ m^{-3}$	$[Mass]_{Seed}$ $\mu g\ m^{-3}$	$[Mass]_{total}$ $\mu g\ m^{-3}$	Vol. SOA (%)	Mass SOA (%)	CE (sdev[a])	f_{44}/f_{57} (sdev[a])
Hydrocarbon standards/reactions											
ER513	02/16/10	azaleic acid	n/a	n/a	n/a	n/a	94.08	n/a	n/a	0.73	2.13
ER527	05/11/10	decane	OH | NO_x	$(NH_4)_2SO_4$	1.33	2.38	33.96	95.37	92.46	0.60	1.50
ER528	05/18/10	undecane	OH | NO_x	$(NH_4)_2SO_4$	0.95	1.69	64.78	98.35	97.32	0.53 (0.14)	1.26 (0.31)
ER522	04/15/10	dodecane	OH | NO_x	$(NH_4)_2SO_4$	0.88	1.58	45.22	97.77	96.37	0.91	0.85
ER529	06/01/10	dodecane	OH | NO_x	$(NH_4)_2SO_4$	2.26	4.04	109.91	97.66	96.19	0.99	0.84
ER530	06/08/10	dodecane	OH | NO_x	$(NH_4)_2SO_4$	1.18	2.11	31.11	95.54	92.74	0.73 (0.07)	1.03 (0.07)
ER523	04/20/10	tridecane	OH | NO_x	$(NH_4)_2SO_4$	0.47	0.85	124.71	99.58	99.32	1.13 (0.01)	0.60 (0.08)
ER545	09/21/10	oleic acid	O_3	$(NH_4)_2SO_4$	1.78	3.18	43.36	95.14	92.09	0.99	0.87
ER547	10/25/10	oleic acid	O_3	$(NH_4)_2SO_4$	1.00	1.79	22.14	94.59	91.20	0.85	0.27
ER518	03/18/10	DOS	n/a	NaCl	0.14	0.31	57.60[b]	99.85[b]	n/a	1.24	0.10
ER519	03/22/10	DOS	n/a	NaCl	0.43	0.92	25.38[b]	98.47[b]	n/a	1.19	0.06
ER548	10/04/10	DOS	n/a	$(NH_4)_2SO_4$	0.10	0.18	37.25	99.70	99.52	1.07	0.06
Biogenic hydrocarbon reactions											
ER501	12/02/09	isoprene	NO_3	$(NH_4)_2SO_4$	3.01	5.39	72.13	95.03	91.92	0.97	2.14
ER534	07/06/10	isoprene	OH | NO_x	$(NH_4)_2SO_4$	1.49	2.66	22.64	91.81	86.67	0.41	3.03
ER535	07/12/10	isoprene	OH	$(NH_4)_2SO_4$	1.46	2.61	30.27	94.19	90.54	0.38 (0.07)	2.50 (0.85)
ER550	10/25/10	isoprene	OH | NO_x	$(NH_4)_2SO_4$	0.76	1.35	25.92	96.62	94.50	0.33 (0.02)	4.55 (0.01)
ER551	11/01/10	isoprene	OH	$(NH_4)_2SO_4$	0.83	1.49	113.42	99.18	98.67	0.35 (0.02)	2.08 (0.07)
ER554	11/17/10	isoprene	OH	$(NH_4)_2SO_4$	0.90	1.61	16.97	93.54	89.49	0.32 (0.02)	3.01 (0.05)
ER502	12/09/09	α-pinene	NO_3	$(NH_4)_2SO_4$	3.01	5.39	109.06	96.81	94.80	0.76 (0.03)	3.74 (0.02)
ER555	11/29/10	α-pinene	OH	$(NH_4)_2SO_4$	0.99	1.78	88.07	98.73	97.94	0.14 (0.02)	6.22 (0.63)
ER558	01/10/11	α-pinene	NO_3	$(NH_4)_2SO_4$	1.29	2.31	132.50	98.91	98.23	0.59 (0.04)	2.87 (0.01)
ER561	01/31/11	β-pinene	NO_3	$(NH_4)_2SO_4$	1.70	3.04	182.92	98.96	98.31	0.56 (0.01)	1.73 (0.05)
ER562	02/08/11	β-pinene	NO_3	$(NH_4)_2SO_4$	1.76	3.15	87.18	97.70	96.25	0.56 (0.08)	2.00 (0.42)
ER503	12/15/09	δ-limonene	NO_3	$(NH_4)_2SO_4$	4.23	7.58	204.45	97.63	96.15	0.30	5.68
ER560	01/24/11	δ-limonene	NO_3	$(NH_4)_2SO_4$	1.76	3.14	94.36	97.88	96.55	0.16 (0.01)	4.82 (0.33)
ER533	06/28/10	β-caryophylene	O_3	$(NH_4)_2SO_4$	1.23	2.19	55.15	97.46	95.86	0.36 (0.01)	2.52 (0.38)
ER563	02/14/11	β-caryophylene	NO_3	$(NH_4)_2SO_4$	1.61	2.88	113.41	98.40	97.39	0.11 (0.03)	2.88 (0.14)
Anthropogenic hydrocarbon reactions											
ER543	09/07/10	benzene	OH | NO_x	$(NH_4)_2SO_4$	1.16	2.08	20.46	93.05	88.69	0.14	15.68
ER544	09/13/10	benzene	OH	$(NH_4)_2SO_4$	2.18	3.90	23.54	87.81	80.16	0.15	13.60
ER540	08/16/10	toluene	OH | NO_x	$(NH_4)_2SO_4$	0.50	0.90	35.74	98.42	97.43	0.19	15.64
ER541	08/23/10	toluene	OH	$(NH_4)_2SO_4$	1.83	3.28	34.19	93.49	89.40	0.12	14.92
ER546	09/27/10	toluene	OH | NO_x	NH_4NO_3	0.11	0.20	62.02	99.80	99.68	0.43 (0.24)	15.72 (0.98)
ER553	11/15/10	toluene	OH	$(NH_4)_2SO_4$	0.43	0.77	42.43	98.86	98.15	0.16 (0.01)	16.61 (0.48)
ER557	12/06/10	toluene	OH | NO_x	$(NH_4)_2SO_4$	0.68	1.22	39.54	98.04	96.81	0.15 (0.01)	26.16 (0.11)
ER536	07/19/10	1,3,5-TMB	OH	$(NH_4)_2SO_4$	1.41	2.52	92.59	98.28	97.21	0.28 (0.10)	4.84 (0.04)
ER538	08/02/10	1,3,5-TMB	OH | NO_x	$(NH_4)_2SO_4$	0.94	1.68	27.08	95.94	93.39	0.37 (0.01)	6.52 (0.09)
ER512	02/08/10	naphthalene	OH | NO_x	$(NH_4)_2SO_4$	0.20	0.36	81.61	99.73	99.56	0.148708	35.64
ER539	08/10/10	naphthalene	OH | NO_x	$(NH_4)_2SO_4$	1.23	2.20	67.91	97.95	96.66	0.18 (0.01)	18.17 (0.71)
ER564	02/22/11	napthalene	NO_3	$(NH_4)_2SO_4$	1.94	3.48	18.99	86.23	77.59	0.18	18.07

[a] Average CE values are reported along with the associated standard deviation for those reactions in which CE was calculated over several different filter sampling intervals.

[b] Calculated from SMPS volume density with ρ_{DOS}=0.917 g cm^{-3}

Table S2. Literature values for chamber-generated SOA density

Reaction System	Average	Reference
α-pinene | O_3	1.198	Zelenyuk et al. (2008)
	1.240	Malloy et al. (2009)
	1.190	Bahreini et al. (2005)
α-pinene | OH | NO_x	1.300	Alfarra et al. (2006)
b-caryophyllene | O_3	1.300	Bahreini et al. (2005)
1,3,5-TMB | OH | NO_x	1.370	Alfarra et al. (2006)

Table S3. OM/OC values calculated from filter samples and AMS

	Hydrocarbon	Oxidant	OM/OC_{fltr}	f_{44} (%)	O/C_{AMS} [a]	OM/OC_{AMS} [b]	OM/OC_{AMS} [c]	OM/OC_{ref}	$OM/OC_{fltr.}/OM/OC_{AMS}$
Hydrocarbon standards/reactions									
ER513	azaleic acid	N/A	2.54	1.36	0.13	1.35	1.33		1.89
ER527	decane	OH | NO_x	3.25	5.55	0.29	1.55	1.65		2.10
ER528	undecane	OH | NO_x	2.66	5.00	0.27	1.52	1.62		1.75
ER522	dodecane	OH | NO_x	1.87	3.80	0.22	1.46	1.55		1.28
ER529	dodecane	OH | NO_x	2.29	3.94	0.23	1.47	1.56		1.56
ER530	dodecane	OH | NO_x	1.87	4.50	0.25	1.50	1.59		1.25
ER523	tridecane	OH | NO_x	2.31	3.21	0.20	1.43	1.53		1.61
ER545	oleic acid	O_3	1.50	3.41	0.21	1.44	1.44		1.04
ER547	oleic acid	O_3	1.47	0.97	0.12	1.33	1.32		1.11
ER518	DOS	N/A	N/A [c]	0.91	0.11	1.32	1.30	1.38 [e]	N/A [d]
ER519	DOS	N/A	N/A [c]	0.85	0.11	1.32	1.30	1.38 [e]	N/A [d]
ER548	DOS	N/A	1.50	0.76	0.11	1.32	1.30	1.38 [e]	1.14
Biogenic hydrocarbon reactions									
ER501	isoprene	NO_3	4.04	2.37	0.17	1.39	2.21		2.90
ER534	isoprene	OH | NO_x	1.22	4.36	0.25	1.49	1.63	1.77 [f]; 1.92-2.00 [g]	0.82
ER535	isoprene	OH	1.44	5.48	0.29	1.54	1.61		0.93
ER550	isoprene	OH | NO_x	2.38	6.89	0.34	1.61	1.90		1.47
ER551	isoprene	OH	2.08	4.58	0.25	1.50	1.59		1.39
ER554	isoprene	OH	2.36	5.55	0.29	1.55	1.63		1.53
ER502	α-pinene	NO_3	2.25	1.69	0.14	1.36	1.57		1.65
ER555	α-pinene	OH	1.69	5.89	0.30	1.56	1.56	1.67 [f]	1.08
ER558	α-pinene	NO_3	1.76	0.43	0.10	1.30	1.43		1.35
ER561	β-pinene	NO_3	1.96	0.64	0.10	1.31	1.50		1.50
ER562	β-pinene	NO_3	1.97	0.78	0.11	1.32	1.52		1.50
ER503	δ-limonene	NO_3	2.69	1.93	0.15	1.37	1.55		1.96
ER560	δ-limonene	NO_3	2.36	3.11	0.20	1.43	1.76		1.65
ER533	β-caryophylene	O_3	1.39	3.48	0.21	1.45	1.45		0.96
ER563	β-caryophylene	NO_3	2.33	2.16	0.16	1.38	1.54		1.69
Anthropogenic hydrocarbon reactions									
ER543	benzene	OH | NO_x	2.73	13.24	0.59	1.92	2.03		1.42
ER544	benzene	OH	2.45	13.64	0.60	1.94	1.99		1.26
ER540	toluene	OH | NO_x	2.48	9.54	0.44	1.74	1.81	1.72 [f]; 2.10-2.15 [g]	1.43
ER541	toluene	OH	2.41	9.25	0.43	1.73	1.76		1.40
ER546	toluene	OH | NO_x	2.32	10.82	0.49	1.80	3.08	1.72 [f]; 2.10-2.15 [g]	1.29
ER553	toluene	OH	2.83	10.80	0.49	1.80	1.83		1.57
ER557	toluene	OH | NO_x	2.46	12.17	0.54	1.87	1.95	1.72 [f]; 2.10-2.15 [g]	1.32
ER536	1,3,5-TMB	OH	1.61	3.78	0.22	1.46	1.46		1.10
ER538	1,3,5-TMB	OH | NO_x	N/A [h]	4.47	0.25	1.49	1.56		N/A [g]
ER512	naphthalene	OH | NO_x	2.34	5.98	0.31	1.57	1.64		1.49
ER539	naphthalene	OH | NO_x	1.71	3.99	0.23	1.47	1.49		1.16
ER564	napthalene	NO_3	3.58	5.06	0.27	1.52	2.05		2.35

[a] $O/C_{AMS} = 0.0382*f_{44}+0.0794$ (Aiken et al., 2008)

[b] $OM/OC_{AMS} = 1.260*O/C_{AMS} + 1.180$ (Aiken et al., 2008)

[c] OM/OC_{AMS} recalculated including AMS NO_3

[d] Filter measurements not available

[e] Calculated from molecular formula

[f] Aiken et al. (2008)

[g] Chhabbra et al. (2009)

[h] Sunset measurements not available